Summer 8-31-2015

Investigation of infinite-dimensional dynamical system models applicable to granular flows

Hao Wu
New Jersey Institute of Technology

Copyright Warning & Restrictions

The copyright law of the United States (Title 17, United States Code) governs the making of photocopies or other reproductions of copyrighted material.

Under certain conditions specified in the law, libraries and archives are authorized to furnish a photocopy or other reproduction. One of these specified conditions is that the photocopy or reproduction is not to be "used for any purpose other than private study, scholarship, or research." If a, user makes a request for, or later uses, a photocopy or reproduction for purposes in excess of "fair use" that user may be liable for copyright infringement,

This institution reserves the right to refuse to accept a copying order if, in its judgment, fulfillment of the order would involve violation of copyright law.

Please Note: The author retains the copyright while the New Jersey Institute of Technology reserves the right to distribute this thesis or dissertation

Printing note: If you do not wish to print this page, then select "Pages from: first page # to: last page #" on the print dialog screen

ABSTRACT

INVESTIGATION OF INFINITE-DIMENSIONAL DYNAMICAL SYSTEM MODELS APPLICABLE TO GRANULAR FLOWS

by
Hao Wu

Recently Blackmore, Samulyak and Rosato developed a class of infinite-dimensional dynamical systems in the form of integro-partial differential equations, which have been called the BSR models. The BSR models were originally derived to model granular flows, but they actually have many additional applications in a variety of fields. BSR models have already been proven to be completely integrable infinite-dimensional Hamiltonian dynamical systems for perfectly elastic interactions in the case of one space dimension, but the well-posedness question of these systems is at least partially answered for the first time here. In particular, dynamical systems of the BSR type are proven to be well posed under mild auxiliary conditions and shown to have interesting properties. Also included is a novel derivation of a formula for (density) wave speeds in flow fields directly from the BSR model. In addition, an innovative semi-discrete numerical scheme for obtaining approximate solutions is described in detail and the questions of consistency, convergence, stability and accuracy of the scheme are treated at considerable length. It is shown how this numerical scheme can be used to help demonstrate the value of these models for predicting the evolution of granular flows and other flow field related phenomena, which is demonstrated to some extent by comparisons of the numerical results with experiments and some DEM simulations.

INVESTIGATION OF INFINITE-DIMENSIONAL DYNAMICAL SYSTEM MODELS APPLICABLE TO GRANULAR FLOWS

by
Hao Wu

A Dissertation
Submitted to the Faculty of
New Jersey Institute of Technology and
Rutgers, The State University of New Jersey – Newark
in Partial Fulfillment of the Requirements for the Degree of
Doctor of Philosophy in Mathematical Sciences

Department of Mathematical Sciences
Department of Mathematics and Computer Science, Rutgers-Newark

August 2015

APPROVAL PAGE

INVESTIGATION OF INFINITE-DIMENSIONAL DYNAMICAL SYSTEM MODELS APPLICABLE TO GRANULAR FLOWS

Hao Wu

Dr. Denis L. Blackmore, Dissertation Advisor — Date
Professor of Mathematics, NJIT

Dr. Anthony D. Rosato, Committee Member — Date
Professor of Mechanical and Industrial Engineering, NJIT

Dr. Lou Kondic, Committee Member — Date
Professor of Mathematics, NJIT

Dr. Linda J. Cummings, Committee Member — Date
Professor of Mathematics, NJIT

Dr. Richard O. Moore, Committee Member — Date
Associate Professor of Mathematics, NJIT

BIOGRAPHICAL SKETCH

Author: Hao Wu

Degree: Doctor of Philosophy

Date: August 2015

Undergraduate and Graduate Education:

- Doctor of Philosophy in Mathematical Sciences,
  New Jersey Institute of Technology, Newark, NJ, 2015
- Master of Science in Pure Mathematics,
  Shandong University, Jinan, China, 2009
- Bachelor of Science in Mathematical Science,
  Shandong University, Jinan, China, 2006

Major: Mathematical Sciences

Presentations and Publications:

A. Rosato, L. Zuo, D. Blackmore, H. Wu, D. Horntrop, D. J. Parker and C. Windows-Yule, "Tapped Granular Column Dynamics: Simulations, Experiments and Modeling" *Computational Particle Mechanics.*

H. Wu, D. Blackmore and A. Rosato, "Global well-posedness of the BSR model for granular flows", In preparation.

H. Wu, D. Blackmore and A. Rosato, "A semi-discrete scheme for the BSR model and other integro-partial differential equations", In preparation.

H. Wu and D. Blackmore, "A Novel Semi-discrete Scheme for a Reduced Continuum Flow Model," *SIAM Dynamical System 2015 Minisymposium*, Snowbird, Utah, May 16-21, 2015.

H. Wu, "Investigation of Infinite-Dimensional Dynamical Systems Models Applicable to Granular Flows," *American Mathematical Society (AMS) - Mathematical Association of American (MAA) Conference Contributed Section*, Baltimore, MD, Jan 15-18, 2014.

H. Wu and D. Blackmore, "Analysis and Simulation of the BSR Model," *SIAM Dynamical System 2013 Minisymposium*, Snowbird, Utah, May 19-23, 2013.

This dissertation is dedicated to my beloved wife and parents

Hao Wu

ACKNOWLEDGMENT

I would like to gratefully and sincerely thank Dr. Denis Blackmore for his guidance, understanding, patience, and most importantly, his friendship during my graduate studies at NJIT. His mentorship was paramount in providing a well rounded experience consistent with my long-term career goals. He encouraged me to not only grow as an mathematician but also as an instructor and an independent thinker. I am not sure many graduate students are given the opportunity to develop their own individuality and self-sufficiency by being allowed to work with such independence. For everything you have done for me, Dr. Blackmore, I thank you.

Special thanks to Drs. Anthony Rosato, Lou Kondic, Linda Cummings and Richard Moore for serving as members of the committee. I would also like to thank the Department of Mathematical Science at NJIT.

My final acknowledgement goes to my wife and parents. Their support always encourages me to move forward.

TABLE OF CONTENTS

TABLE OF CONTENTS
(Continued)

Chapter **Page**

LIST OF FIGURES

LIST OF FIGURES
(Continued)

Figure **Page**

CHAPTER 1

INTRODUCTION

1.1 Overview

Granular materials are quite common in nature. This is evident in the granular structure in collections of nuts, coal, sand, rice, coffee, fertilizer, ball bearings and many other materials. They are commercially important in applications as diverse as pharmaceutics, agriculture, and energy production. In industry, tons of raw materials are handled and processed daily to produce goods in everyday use. Industrial processes developed to work with bulk solids generally require various systems that are used to transport and manipulate the material (for example [21, 28]).

Figure 1.1 Some examples of granular materials.

Although granular material is everywhere and very important in everyday life, granular phenomena are still very far from being well understood. Generally speaking, granular material is a collection of distinct macroscopic particles. The evolution of the particles follows Newton's classical equations, with interaction forces between

particles that are not zero only when there is a contact between them. Although granular materials are very simple to describe, they exhibit a tremendous amount of complex behavior; and most of these behavior has not yet been explained in a satisfactory manner. They behave differently than solids, liquids and gases. Indeed, in comparison to the well-understood behavior of fluids, gases and solids, for which there are many reliable applicable predictive mathematical models, the science of granular materials is really still in its infancy [32]; this has led many scientists to characterize granular materials as a new form of matter.

Research on granular materials can be traced back at least to Charles-Augustin de Coulomb, whose law of friction was originally stated for granular materials. In the 1930s, Ralph Alger Bagnold was amazed by sand dunes during his explorations of the Libyan desert and wrote a book "The Physics of Blown Sand and Sand Dunes" [3], which still remains an important reference to this day. Since then, various communities, like mathematics, engineering and physics, have paid tremendous effort to understand the behavior of granular systems.

In the Summer of 1953, Fermi, Pasta, Ulam and Tsingou conducted numerical experiments of a vibrating string that included a non-linear term. They found the system exhibited a very complicated quasi-periodic behavior, and then published their results in a Los Alamos technical report in 1955 [18], which is known as the FPU problem. The equation for their model has been proved to be equivalent to KdV equation in the long-wave continuum limit [35, 57]. Their work directly inspired granular studies using an FPU-chain type approach. Along this line, there is a direct lattice-dynamics FPU-chain type approach by Sen, Manciu [43, 44] and others, which deals directly with the particle dynamics.

A successful continuum description of granular media could exploit the powerful methods of standard fluid dynamics to describe a variety of granular flow phenomena, but the validity of a continuum description of granular materials has been questioned

and remains an open problem. In this regard, one should mention that the long-wave limit procedure has been applied to particle dynamics with some success to obtain partial differential equation (PDE) models by researchers such as Nesterenko, Daraio et al [15, 36, 37].

During the last few years, Behringer, Kondic, Rosato and others developed a variety of discrete element 2D and 3D molecular dynamical simulations with the goal of explaining some basic features of statics and dynamics of granular materials [12, 33, 41, 51]. Evolution of force networks in granular systems are also deeply investigated by Kondic, Kramar and others [22, 23, 24, 25]. There are also other groups such as Swinney et al. [7] that have obtained numerical solutions of continuum equations of the Navier-Stokes type for the vertically oscillated granular layers problem. In addition, there have been numerous experimental investigations of oscillating granular configurations such as [8, 17, 29, 30].

Granular flow dynamics is now very widely studied using many different approaches. Even when it comes to the field of the dynamical behavior of configurations of particles subjected to small periodic tapping forces, there are several extant explanations. Actually, one can use the framework of Newton's second law (if rotations are ignored and the Newton–Euler equations if they are not) to construct a model, which is a system of second-order differential (momentum) equations applied to every single particle, to describe the tapping dynamics of a column or a 3D container. However, it is difficult both analytically and numerically to determine the important flow properties such as the density and velocity field evolution. Moreover, the inherent disorder present in granular systems is a further complication that always affects the energy and density propagation through the medium.

1.2 Objective

This research is focused primarily on explaining the dynamical behavior of configurations of particles subjected to small tapping forces. In [5], Blackmore, Samulyak and Rosato used fundamental physics principles to derive an integro-partial differential equation model for granular dynamics, which shares some features with models derived using the long-wave limit. This system is now called the BSR model. It is an infinite-dimensional nonlinear dynamical system that is relatively amenable to analysis and has proven to be capable of predicting some of the most important aspects of the evolution of density and velocity fields with acceptable accuracy [4, 6, 42].

The primary objective of this dissertation is to prove the well-posedness of BSR model under physically reasonable mathematical restrictions, and then develop, analyze and implement a novel semidiscrete numerical scheme incorporating moving averages to analyze the dynamics of a granular column, with particular attention to how the density field and velocity field evolve with respect to time. It appears that the well-posedness result presented is the first to appear in the literature for any realistic continuum model of granular flows and the semidiscrete numerical scheme is at least as effective and efficient as any that are currently available for such models. With respect to the evolution of the density, some special attention is given to density wave propagation; in fact, a novel derivation of density wave propagation speed is obtained directly from the BSR equations. Finally, several comparisons of (approximate numerical) solutions obtained from the BSR model are made with DEM simulations and experiments to confirm the efficacy of the BSR approach.

1.3 Outline of Dissertation

The exposition begins in Chapter 2 with a quick review of the BSR model. A brief description of the form of the BSR equation in Euclidean n-space $\mathbb{R}^n$ is provided

along with a succinct explanation of how it, as an integro-partial differential equation (IPDE), can be used to model the evolution of rather general particle configurations in finite-dimensional spaces.

In Chapter 3, the main analytical result is presented, namely, a proof of the well-posedness of BSR model under mild, physically realistic conditions. The method and tools employed in the proof are analogous to those used to obtain similar results for the Boltzmann–Enskog equation [10, 16, 19, 38, 52], but they are different in many respects.

In Chapter 4, attention is turned to describe the semidiscrete numerical approach to solve the BSR system equations. The potential applicability of the numerical scheme is illustrated by implementing the code for the case of an oscillating column of particles. Simulations results are displayed and comparisons between the semidiscrete approach and discrete element simulation are discussed.

In Chapter 5, a convergence study showing the asymptotic rate of error is given; and a rather detailed von Neumann stability analysis is presented to investigate the linearized frozen coefficients BSR system in one space dimension.

In Chapter 6, a summary of the work is presented along with a description of some related prior research. Also included is an outline of some plans for future research aimed at extending, generalizing and improving the results presented in this dissertation.

Finally, a novel derivation of local wave speed, a review of the Runge-Kutta method and a pseudo-code for the semidiscrete numerical scheme are provided in the Appendix.

CHAPTER 2

PRELIMINARIES

A description of how the BSR integro-partial differential equation (IPDE) can be used to model the evolution of rather general particle configurations in spaces of finite dimension will be given in this section. The BSR model system in Euclidean n-space $\mathbb{R}^n$ has the form

$$\begin{aligned} &\frac{\partial u_i}{\partial t} + u_1 \frac{\partial u_i}{\partial x_1} + \cdots + u_n \frac{\partial u_i}{\partial x_n} \\ &\quad = F_i \left(t, x_1, \ldots, x_n, u_1, \ldots, u_n, \partial_{x_1} u_1, \ldots, \partial_{x_n} u_1, \ldots, \partial_{x_1} u_n, \ldots, \partial_{x_n} u_n\right), \end{aligned} \tag{2.1}$$

for $1 \leq i \leq n$, where t is the evolution parameter (time), $\boldsymbol{x} := (x_1, \ldots, x_n) \in \mathbb{R}^n$ represents a point in space, $\boldsymbol{u} = \boldsymbol{u}(\boldsymbol{x}, t) := (u_1, \ldots, u_n) = (u_1(\boldsymbol{x}, t), \ldots, u_n(\boldsymbol{x}, t)) \in \mathbb{R}^n$ is the velocity field that determines the motion of the particles via

$$\dot{\boldsymbol{x}} = \boldsymbol{u}(\boldsymbol{x}, t), \tag{2.2}$$

$\partial_{\boldsymbol{x}} u_i := (\partial_{x_1} u_i, \ldots, \partial_{x_n} u_i) \in \mathbb{R}^n$, and the F_i represent the externally applied and internal interaction force per unit mass components at each point, $1 \leq i \leq n$. System (2.1) can be recast in a much more concise form by introducing the additional notation including the $n \times n$ matrix $\boldsymbol{u}_{\boldsymbol{x}} := (\partial u_i / \partial x_j) \in \mathbb{R}^{n \times n}$ and $\boldsymbol{F} := (F_1, \ldots, F_n)$; namely,

$$\boldsymbol{u}_t + \boldsymbol{u}_{\boldsymbol{x}} \boldsymbol{u} = \boldsymbol{F}\left(t, \boldsymbol{x}, \boldsymbol{u}, \boldsymbol{u}_{\boldsymbol{x}}\right). \tag{2.3}$$

Here

$$\boldsymbol{F} : [0, \infty) \times \Omega_t \times \boldsymbol{u}\left(\Omega_t\right) \times \boldsymbol{u}_{\boldsymbol{x}}\left(\Omega_t\right) \to \mathbb{R}^n$$

is a smooth ($= C^\infty$) function, and the subscript t on the "physical domain" Ω_t of $(t, \boldsymbol{x})$ variables indicates that it may vary with time due to prescribed motions applied

to its boundary $\partial\Omega_t$. At this point it is instructive to note that in order to obtain unique solutions to (2.3) it is necessary to prescribe auxiliary conditions such as the initial velocity on the boundary of the domain in a form such as

$$\boldsymbol{u}(\boldsymbol{x}, 0) = U(\boldsymbol{x}) \text{ for } x \in \partial\Omega_0.$$

Next, additional details shall be provided concerning the nature of $\boldsymbol{F}$ and other aspects of the BSR model. In the context of modeling flows, the BSR model has the more specific form given by the IPDE

$$\begin{aligned} \boldsymbol{u}_t + \boldsymbol{u}_{\boldsymbol{x}}\boldsymbol{u} &= \boldsymbol{F}(t, \boldsymbol{x}, \boldsymbol{u}, \boldsymbol{u}_{\boldsymbol{x}}) \\ &:= \boldsymbol{E}(t, \boldsymbol{x}, \boldsymbol{u}, \boldsymbol{u}_{\boldsymbol{x}}) + \int_{B_r(\boldsymbol{x})} \kappa\left(t, \boldsymbol{x}, \boldsymbol{y}, \boldsymbol{u}, \boldsymbol{u}_{\boldsymbol{x}}\right) \boldsymbol{\Theta}\left(\boldsymbol{x}, \boldsymbol{y}, \boldsymbol{u}(\boldsymbol{y}, t) - \boldsymbol{u}(\boldsymbol{x}, t)\right) d\boldsymbol{y}, \end{aligned} \tag{2.4}$$

for $(t, \boldsymbol{x}) \in [0, \infty) \times \Omega_t$, together with the initial condition

$$\boldsymbol{u}(\boldsymbol{x}, 0) = U(\boldsymbol{x}) \text{ for } \boldsymbol{x} \in \Omega_0. \tag{2.5}$$

Here $\boldsymbol{E}$ is the external force per unit mass (on a particle), and the integral represents the interior (interaction) force per unit particle, which naturally depends on the distribution of nearby particles and their velocities as well as any parts of the boundary with which the particle is interacting. External forces may be due to a gravitational, electromagnetic or imposed flow field or a combination thereof, but in most cases only gravitational forces are present. The integral is over a standard Euclidean closed ball of radius r centered at $\boldsymbol{x}$, κ is a smooth function representing the distribution of particles and their velocities throughout the ball (which is taken to be proportional to the density), and $\boldsymbol{\Theta}$ is the smooth vector-valued interaction force among particles (and possibly physical boundaries) within the ball, which

may be taken as any of the standard models such as Hertzian, Walton–Braun, Walton–Braun–Mindlin–Deresewicz or any of their variations [34, 54, 55].

CHAPTER 3

ANALYSIS OF BSR MODEL

3.1 Introduction

Unlike fluid dynamics that can be successfully modeled in almost all respects by the Navier–Stokes equations, granular flows appear not to have anything resembling a universally reliable mathematical model capable of accurately and efficiently predicting the associated dynamical phenomenal across a wide swath of flow regimes and constituent configurations. Consequently, the search for effective mathematical models for particle dynamics has continued and still continues to be an active area of research within engineering, applied dynamical systems and physics communities. That is not to say that there have not been many important advances in the state-of-the-art as a result of this substantial research activity over the last several decades, only that the search for a reasonable analog of the Navier–Stokes equations for granular flows is far from reaching an acceptable conclusion. In fact, it is still safe to say that simulation and experimental investigations such as those in [8, 4, 11, 12, 17, 29, 33, 42, 41, 48, 50] are the most reliable means of predicting and interpreting particle dynamics in a majority of cases. It is this search for an effective mathematically tractable model capturing most of the inherent fundamental principles of physics associated with granular dynamics that led to the development of the Blackmore–Samulyak–Rosato (BSR) model [5] comprising a system of integro-partial differential equations (IPDEs). Since its introduction, not only has the BSR model proved to be rather successful in dealing with a variety of granular flow regimes [4, 6, 42], it has also been observed to be capable of handling many other types of flow fields characterizing phenomena ranging from the microscopic to the macroscopic.

The search for mathematical models for granular flows has for the most part followed two roads (which have some natural crossroads) : continuum models inspired by the Navier–Stokes equations or derived from long-wave limits of many-particle classical evolution equations; and direct lattice dynamics approaches having their roots in the Fermi–Pasta–Ulam problem [18]. Among the more successful Navier–Stokes inspired models have been those investigated by Behringer, Kondic, Pöschel, Swinney and their collaborators such as in [7, 9, 12, 33, 51]. The continuum models in these investigations have generally employed some analytical tools, mainly of the asymptotic variety, but in most instances numerical methods were used to study the dynamics. On the other hand, researchers such as Nesterenko, Daraio and their collaborators used long-wave limits to pass from lattice type dynamical systems to continuum models from which they extracted useful information about certain granular flows, which they were in some cases actually able to verify experimentally [15, 36, 37]. For example, Nesterenko [36] showed that certain long-wave continuum models of one-dimensional particle configurations interacting via the perfectly elastic Hertzian model are completely integrable, possessing soliton solutions that can be verified experimentally. It is interesting to note that an analogous complete integrability result was proved for the BSR model for one-dimensional particle dynamics under the assumption of perfectly elastic particle-particle and particle-boundary interactions [6].

There is a very definite, direct link between Nesterenko's integrability results and the pioneering (essentially one-dimensional lattice dynamics) study of Fermi, Pasta and Ulam [18] that led to the long-wave continuum limit that was shown to be equivalent to the KdV equation by Zabusky and Kruskal [57] , which was instrumental in the development of the integrability theory of infinite-dimensional Hamiltonian dynamical systems. The FPU - Zabusky–Kruskal - Nesterenko connection is one of the most famous and important examples of the cross-fertilization between lattice

and infinite-dimensional continuum dynamics, but it is possible to study each of these types of systems more or less independently and still extract useful information about the phenomena being modeled. For example, there is the direct lattice-dynamics FPU-chain type approach by Sen and Manciu [43, 44], among others, dealing directly with the particle dynamics that has been rather successful in predicting such behavior as steady-state solutions and traveling waves in some granular flow regimes.

In what follows, the exposition begins with a brief description of the derivation of the BSR model in Euclidean n-space $\mathbb{R}^n$, noting that full details can be found in [5]. In addition, various formulations of the model are discussed with the aim of showing how this IPDE can be used to model the evolution of rather general particle configurations in finite-dimensional spaces. This is followed by a proof of the well-posedness of the BSR systems under rather mild assumptions when it comes to tapping problems and other particulate dynamics regimes that are of interest to the applied granular flow communities.

3.2 Derivation and Formulations of the BSR Model

The BSR equations were originally developed as an approximate limiting continuum (integro-PDE) model for granular flows, but they also can serve as approximate models for almost any type of fluid flow, including superfluid and MHD flows. In particular, the initial work was inspired by the problem of predicting the motion of a large number of granular particles in a vibrating container as illustrated in Figure 3.1.

Figure 3.2 provides a more general intuitive idea for the limiting basis of the model.

As indicated above, the derivation will be confined to Euclidean n-space $\mathbb{R}^n := \{\boldsymbol{x} := (x_1, \ldots, x_n) : x_k \in \mathbb{R}, 1 \leq k \leq n\}$. In this regard there are several points worthy of note: In almost all applications, the dimension $n = 1, 2$ or 3, but the

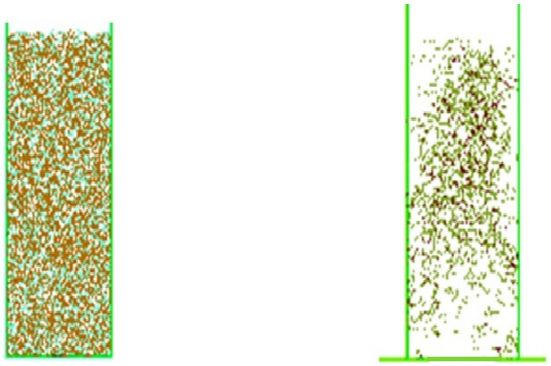

Figure 3.1 Particles in a vibrating container.

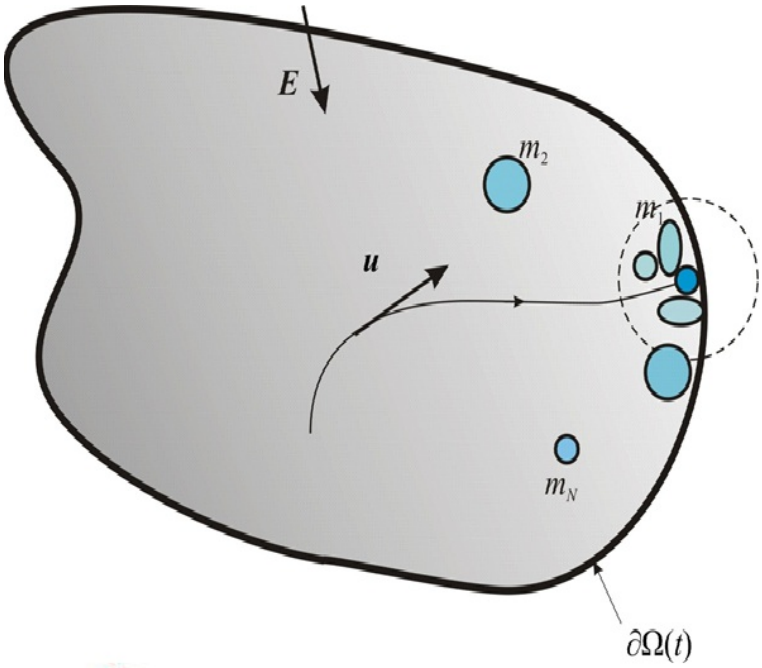

Figure 3.2 Intuitive basis for the BSR equation.

derivation and analysis are essentially the same for all finite-dimensional Euclidean spaces and one can envisage possible applications in spaces of dimension greater than than three. The BSR model can also be generalized to smooth finite-dimensional Riemann manifolds without much difficulty for those familiar with the fundamentals of differential geometry. There are applications in which such a generalization would be useful, but since they are not treated in this thesis, it was decided to simply omit them in the sequel.

The derivations begins with the classical equations of motion for N particles having masses $m_1, \ldots, m_N$, where N is a natural number several orders of magnitude greater than one ($N \gg 1$) located, respectively at points $\boldsymbol{q}_1, \ldots, \boldsymbol{q}_N$ in $\mathbb{R}^n$. The equations of motion for the evolution of the particles follow the Newton's second law ordinary differential equations (ODEs)

$$m_i \ddot{\boldsymbol{q}}_i = \boldsymbol{E}_i(\boldsymbol{q}_i, \dot{\boldsymbol{q}}_i, t) + \sum\nolimits_{j=1}^{k(i)} \boldsymbol{F}_{ij}\left(\boldsymbol{q}_j, \dot{\boldsymbol{q}}_j, t\right), \ (1 \leq i \leq N), \tag{3.1}$$

where the dot over the (vector) variables denotes d/dt, $\boldsymbol{E}_i$ is the external force on m_i, which might be just gravity or an electromagnetic force or any other force acting on each particle in the medium and the F_{ij} are interaction forces on m_i due to the other particles (usually just those in close proximity) or interactions with the material portions of the domain Ω of the particle configuration, denoted as $\partial\hat{\Omega}$, which might be moving with time. Dividing each (3.1) by m_i yields

$$\begin{aligned} \ddot{\boldsymbol{q}}_i &= \boldsymbol{e}_i(\boldsymbol{q}_i, \dot{\boldsymbol{q}}_i, t) + \sum\nolimits_{j=1}^{l(i)} \left(m_j/m_i\right) m_j^{-1} \boldsymbol{F}_{ij}\left(\boldsymbol{q}_j, \dot{\boldsymbol{q}}_j, t\right) \\ &= \boldsymbol{e}_i(\boldsymbol{q}_i, \dot{\boldsymbol{q}}_i, t) + \sum\nolimits_{j=1}^{k(i)} \left(m_j/m_i\right) \boldsymbol{f}_{ij}\left(\boldsymbol{q}_j, \dot{\boldsymbol{q}}_j, t\right), \ (1 \leq i \leq N), \end{aligned} \tag{3.2}$$

where e_i and f_{ij} represent the external and interaction forces, respectively, per unit mass on m_i.

To complete the derivation of the BSR momentum equation, the Newtonian formulation of (3.2) is converted to transport form in which each particle is followed

along the trajectory. Then the limit is computed as the number of particles $N \to \infty$, which when applied to the summations of the interaction forces in the above equations can be interpreted as an averaged integral of the forces per unit mass. Whence, if the distribution of particles $\delta = \delta(\boldsymbol{x}, t)$ is known in advance and it is assumed that only particles and material boundary elements within a ball of radius r (> 0), denoted as $B_r(\boldsymbol{x}) = \{\boldsymbol{y} \in \mathbb{R}^n : |\boldsymbol{y} - \boldsymbol{x}| \leq r\}$, where $|\cdot|$ is the standard Euclidean norm in $\mathbb{R}^n$, interact with any given point, this procedure leads to the momentum equation (system) of the BSR model (cf. [5]) given as

$$\begin{aligned} \frac{\partial u_k}{\partial t} + u_1 \frac{\partial u_k}{\partial x_1} + \cdots + u_n \frac{\partial u_k}{\partial x_n} = \Psi_k &:= e_k(t, \boldsymbol{x}, \boldsymbol{u}) \\ &+ \frac{1}{\operatorname{vol} B_r(\boldsymbol{x})} \int_{B_r(\boldsymbol{x})} \delta(\boldsymbol{y}, t) \theta_k(\boldsymbol{x}, \boldsymbol{y}, \boldsymbol{u}(\boldsymbol{x}, t), \boldsymbol{u}(\boldsymbol{y}, t)) d\boldsymbol{y}, \end{aligned} \tag{3.3}$$

for $1 \leq k \leq n$, where $\boldsymbol{u} = \boldsymbol{u}(\boldsymbol{x}, t) := (u_1, \ldots, u_n) = (u_1(\boldsymbol{x}, t), \ldots, u_n(\boldsymbol{x}, t)) \in \mathbb{R}^n$ is the velocity field that determines the motion of the particles via

$$\dot{\boldsymbol{x}} = \boldsymbol{u}(\boldsymbol{x}, t), \tag{3.4}$$

e_k is the k^{th} component of the external force per unit mass $\boldsymbol{e} := (e_1, \ldots, e_n) \in \mathbb{R}^n$, θ_k is the k^{th} component of the interaction force per unit mass $\boldsymbol{\Theta} := (\theta_1, \ldots, \theta_n) \in \mathbb{R}^n$ and Ψ_k is the k^{th} component of the total force per unit mass $\boldsymbol{\Psi} := (\Psi_k, \ldots, \Psi_k) \in \mathbb{R}^n$.

The system (3.3) comprising the BSR momentum equation can be written in a far more concise vector form by introducing some fairly standard vector notation. In particular, define $\boldsymbol{u}_{\boldsymbol{x}}$ to be $n \times n$ matrix $\boldsymbol{u}_{\boldsymbol{x}} := (\partial u_i / \partial x_j) \in \mathbb{R}^{n \times n}$, let the operator ∇ be defined as usual for both real and vector-valued functions and $< \cdot, \cdot >$ denote the standard inner (dot) product in $\mathbb{R}^n$, then (3.3) can be recast as

$$\begin{aligned} \boldsymbol{u}_t + \boldsymbol{u}_{\boldsymbol{x}} \boldsymbol{u} = \boldsymbol{u}_t + \langle \boldsymbol{u}, \nabla \rangle \boldsymbol{u} = \ & \boldsymbol{\Phi}(t, \boldsymbol{x}, \boldsymbol{u}, \boldsymbol{u}_{\boldsymbol{x}}) \\ &= \boldsymbol{e}(\boldsymbol{x}, \boldsymbol{u}, t) + \int_{B_r(\boldsymbol{x})} \hat{\delta}(\boldsymbol{y}, t) \boldsymbol{\Theta}(\boldsymbol{x}, \boldsymbol{y}, \boldsymbol{u}(\boldsymbol{x}, t), \boldsymbol{u}(\boldsymbol{y}, t)) d\boldsymbol{y}, \end{aligned} \tag{3.5}$$

where $\hat{\delta} := \delta/\mathrm{vol}\, B_r(\boldsymbol{x})$ is the particle distribution per unit volume. Here

$$\boldsymbol{\Phi} : [0,\infty) \times \Omega_t \times \boldsymbol{u}\,(\Omega_t) \times \boldsymbol{u}_{\boldsymbol{x}}\,(\Omega_t) \to \mathbb{R}^n$$

is assumed to be a smooth ($= C^\infty$) function, and the subscript t on the "physical domain" Ω_t of $(t, \boldsymbol{x})$ variables indicates that it may vary with time due to prescribed motions applied to its boundary $\partial\Omega_t$. At this point it is instructive to note that in order to obtain unique solutions to (3.5), it is necessary to prescribe auxiliary conditions such as the initial velocity on the boundary of the domain in a form such as

$$\boldsymbol{u}(\boldsymbol{x}, 0) = \boldsymbol{u}_0(\boldsymbol{x}) \text{ for } \boldsymbol{x} \in \Omega_0. \tag{3.6}$$

A few words are in order concerning the BSR momentum equation (3.5). The integral on the right-hand side represents the interior (interaction) force per unit mass, which naturally depends on the distribution of nearby particles and their velocities as well as any parts of the boundary with which the particle is interacting. This representation in terms of a local integral is appropriate when the interaction forces at a point are a result of just nearby particles, such as those caused by collisions only, which is the type studied in this thesis. However, in other applications the interactions may be due to forces at a distance as it would be in the case of charged particles, and then the integrals would have to be global or at least over larger regions in which the interaction forces are not negligible. External forces may be due to any number of phenomena, including gravitational, electromagnetic or an imposed flow field of the ambient medium or a combination thereof, but in most cases only gravitational forces are present. In the sequel, it shall be assumed that the external force field is independent of the particle velocity field, so that it depends only on $(\boldsymbol{x}, t)$. The interaction (vector) force kernel $\boldsymbol{\Theta}$ is the smooth vector-valued interaction force among particles (and possibly physical boundaries) within the ball $B_r(\boldsymbol{x})$ which may

be taken as any of the standard models such as Hertzian (such as in [15, 18, 36, 37, 43, 44]), Walton–Braun, Walton–Braun–Mindlin–Deresewicz [34, 55] or any of their variations such as those in [4, 5, 6]. The Hertzian interaction force model is nonlinear and depends only on particle separation, but the interactions are perfectly elastic, which means that there is no diminution of energy in the collisions. In contrast, most of the other standard models in use are designed for collisions that are not perfectly elastic, depend on the velocity and entail energy loss. For the velocity dependent interaction force model, it is usually necessary to include a compensatory scaling to balance the right-hand side of (3.5) to zero if the configuration starts at equilibrium. Finally, it is interesting to note that it was shown in [5] that a Taylor series approximation of the integral term actually yield the momentum component of the Navier–Stokes equations, which can be viewed as something of a confirmation of the validity of the BSR model.

3.2.1 Derivation of the Complete BSR Model

If the volumetric distribution kernel $\hat{\delta}$ is known in advance, the initial value problem (IVP) expressed as (3.5)-(3.6) would - at least in principle - completely determine the dynamics of the system. However, the distribution is almost never a priori known, so another equation is required. The most obvious choice for the volumetric distribution is a scaled version of the density ρ, which is to be denoted by $\hat{\rho} := \lambda\rho$, where λ is a constant having units of $mass^{-1}$ so that multiplication by λ may be viewed as division by a fixed reference mass. With these observations, the complete BSR model takes the form of (3.5) together with the continuity equation and the associated initial values; namely,

$$\boldsymbol{u}_t + \langle \boldsymbol{u}, \nabla \rangle \, \boldsymbol{u} = \boldsymbol{e}(\boldsymbol{x}, t) + \int_{B_r(x)} \hat{\rho}(\boldsymbol{y}, t) \boldsymbol{\Theta}(\boldsymbol{x}, \boldsymbol{y}, \boldsymbol{u}(\boldsymbol{x}, t), \boldsymbol{u}(\boldsymbol{y}, t)) d\boldsymbol{y}, \tag{3.7}$$

$$\rho_t + \langle \boldsymbol{u}, \nabla \rangle \rho = -\rho \mathrm{tr} \boldsymbol{u}_{\boldsymbol{x}} = -\rho \mathrm{div} \boldsymbol{u}, \tag{3.8}$$

together with the initial conditions

$$\boldsymbol{u}(\boldsymbol{x}, 0) = \boldsymbol{u}_0(\boldsymbol{x}), \rho(\boldsymbol{x}, 0) = \rho_0(\boldsymbol{x}), \ \boldsymbol{x} \in \Omega_0, \tag{3.9}$$

where tr is the standard trace operator applied to the matrix $\boldsymbol{u}_{\boldsymbol{x}}$, which is equal to the divergence of $\boldsymbol{u}$, denoted as usual by div $\boldsymbol{u} = \langle \nabla, \boldsymbol{u} \rangle$. The domain of this system, $M := \{(\boldsymbol{x}, t) : (\boldsymbol{x}, t) \in \Omega_t \times t, t \geq 0\}$, is assumed to be a smooth ($= C^\infty$) submanifold of $\mathbb{R}^n \times [0, \infty) \subset \mathbb{R}^{n+1}$ as are the prescribed functions $\boldsymbol{e}, \boldsymbol{\Theta}, \boldsymbol{u}_0$ and ρ_0.

It is worth noting that equations (3.7),(3.8) and (3.9) can be recast in an equivalent non-local form as follows: Assume for the moment that $\boldsymbol{u}$ is a known smooth function, then (3.8) is a quasilinear equation that can be solved by characteristics to obtain

$$\rho(\boldsymbol{x}, t) = \psi(\boldsymbol{\phi}(0; \boldsymbol{x}, t)) \exp\{-\int_0^t \mathrm{tr} \boldsymbol{u}_x(\boldsymbol{\phi}(\tau; \boldsymbol{\phi}(0; \boldsymbol{x}, t), 0), \tau) d\tau \tag{3.10}$$

where $\boldsymbol{\phi}(t; \boldsymbol{x}_0, t_0)$ is the "unique" solution of the ODE-IVP

$$\dot{\boldsymbol{x}} = \boldsymbol{u}(\boldsymbol{x}, t) \tag{3.11}$$

$$\boldsymbol{x}(t_0) = \boldsymbol{x}_0 \tag{3.12}$$

supplemented by the ODE-IVP (3.11)-(3.12), where ρ (and so also $\hat{\rho}$ is given by (3.10).

3.2.2 Reformulation in Moving Coordinates

It is often useful to reformulate (3.7)-(3.9) in a coordinate system moving with the applied motion so that the space domain Ω_t remains constant. This can be easily done

in the special case where the applied motion depends only on time and possibly some parameters; for example if it is of the form (in terms of the original fixed Euclidean coordinates)

$$\boldsymbol{x} = \boldsymbol{\vartheta}\left(t; \boldsymbol{\mu}\right), \tag{3.13}$$

where $\boldsymbol{\vartheta}$ is a smooth, typically oscillatory function of time and possibly a parameter (vector) $\boldsymbol{\mu} \in \mathbb{R}^m$. Now define new inertial coordinates moving with the applied motion as follows:

$$\boldsymbol{z} := \boldsymbol{x} - \boldsymbol{\vartheta}\left(t; \boldsymbol{\mu}\right). \tag{3.14}$$

Then, the corresponding velocity field dynamics is described by the IVP

$$\dot{\boldsymbol{z}} = \dot{\boldsymbol{x}} - \dot{\boldsymbol{\vartheta}} = \boldsymbol{w}\left(\boldsymbol{z}, t\right) := \boldsymbol{u}\left(\boldsymbol{x} + \boldsymbol{\vartheta}, t\right) - \dot{\boldsymbol{\vartheta}}, \quad \boldsymbol{z}(t_0) = \boldsymbol{x}_0 - \boldsymbol{\vartheta}\left(t_0; \boldsymbol{\mu}\right), \tag{3.15}$$

It is easy to show by making extensive use of the chain rule that the moving coordinate analog of the IVP for the momentum equation is

$$\begin{aligned} \boldsymbol{w}_t + \boldsymbol{w}_{\boldsymbol{z}}\boldsymbol{w} &= -\ddot{\boldsymbol{\vartheta}}\left(t; \boldsymbol{\mu}\right) + \boldsymbol{\Phi}\left(t, \boldsymbol{z} + \boldsymbol{\vartheta}, \boldsymbol{w} + \dot{\boldsymbol{\vartheta}}, \boldsymbol{w}_{\boldsymbol{z}}\right), \\ \boldsymbol{w}(\boldsymbol{z}, 0) &= \boldsymbol{w}_0(\boldsymbol{z}) := \boldsymbol{u}_0\left(\boldsymbol{z} + \boldsymbol{\vartheta}(0; \boldsymbol{\mu})\right) - \dot{\boldsymbol{\vartheta}}(0; \boldsymbol{\mu}), \end{aligned} \tag{3.16}$$

so the primary changes are in the expected addition of the inertial acceleration $-\ddot{\boldsymbol{\vartheta}}\left(t; \boldsymbol{\mu}\right)$ and the translation of the initial velocity field. Consequently, in most cases of interest, where the interaction force model is velocity translation invariant, one can use the original symbols for the moving coordinates and simply add an inertial acceleration and make a translation of the initial velocity.

Furthermore, it is a simple matter to verify that the continuity equation is invariant under the change to the moving coordinates; namely, it is just

$$\rho_t + \langle \boldsymbol{w}, \nabla\rho \rangle = -\rho \mathrm{tr}\boldsymbol{w}_{\boldsymbol{z}} = -\rho \mathrm{div}\boldsymbol{w}, \quad \rho(\boldsymbol{z}, 0) = R(\boldsymbol{z}). \tag{3.17}$$

It should be noted that if one is dealing with an applied motion that is a function only of time, as is the case in the tapping and oscillating floor problems, it is actually necessary to convert the system to moving a moving coordinate frame as in (3.16)-(3.17) in order to maintain it as an IVP. Moreover, the coordinate transformation approach can also be used when the applied motion depends on the position as well as the time, but this would result in more significant changes in the governing equations.

3.3 Well-posedness of the BSR Model

In this section, the following properties - comprising what is known as well-posedness - of the complete BSR model IPDE-IVP shall be proved under only mildly restrictive assumptions, which are to be delineated in the sequel. Although the proof of the main theorem employs analytic techniques used for the analysis of quasilinear hyperbolic systems (see e.g. [31]) and shares some features with existence (both local and global) and uniqueness arguments in the literature for the Boltzmann and Boltzmann-Enskog equations such as in [10, 16, 19, 38, 52], it is quite novel inasmuch as it is based on the method of characteristics, the fundamentals of which may be found in many introductory treatments of partial differential equations such McOwen [31] and Renardy and Rogers [40]. Moreover, it appears to be the only extant result of its kind for relatively realistic continuum mathematical models of granular flow dynamics.

(W1) There exists a global solution.

(W2) The solution is unique.

(W3) The solution depends continuously on initial conditions and parameters.

These properties shall be proved for the following system, which based on the above discussion subsumes the complete BSR model if the interaction kernel is velocity translation invariant and any applied motion depends only on the time t and possibly a parameter vector μ :

$$\begin{aligned} \boldsymbol{u}_t &= \boldsymbol{\alpha}\left(\boldsymbol{x}, t; \boldsymbol{\mu}\right) - \langle \boldsymbol{u}, \nabla \rangle \boldsymbol{u} + \int_{B_r(\boldsymbol{x})} \rho(\boldsymbol{y}, t) \boldsymbol{\Theta}\left(\boldsymbol{x}, \boldsymbol{y}, \boldsymbol{u}(\boldsymbol{x}, t), \boldsymbol{u}(\boldsymbol{y}, t)\right) d\boldsymbol{y}, \\ \rho_t &= -\left[\langle u, \nabla \rangle \rho + \rho \operatorname{div} \boldsymbol{u}\right], \end{aligned} \tag{3.18}$$

which is subject to the initial conditions

$$\boldsymbol{u}(\boldsymbol{x}, 0) = \boldsymbol{u}_0(\boldsymbol{x}), \rho(\boldsymbol{x}, 0) = \rho_0(\boldsymbol{x}), \ \boldsymbol{x} \in \Omega, \tag{3.19}$$

where Ω is a fixed, smooth submanifold of $\mathbb{R}^n$ with boundary $\partial\Omega$ and the system is defined for $\Omega \times [0, \infty)$. Here the function $\boldsymbol{\alpha}$ represents the external and any inertial forces present, and the circumflex over the density ρ has been omitted since the normalizing constant can be assumed to be absorbed into the interaction force kernel.

3.3.1 Observations Concerning the Method of Characteristics

As indicated, the global well-posedness proof to be presented in what follows is to be based on the method of characteristics, which to those familiar with the technique might seem to be counter-intuitive. After all, although the method might work locally for non-characteristic initial data, it often leads to gradient catastrophes indicative of shocks or multiple solutions in the large (as shown in the next simplified example of a one-dimensional granular flow model), thereby rendering it useless as an approach to proving global well-posedness.

Example A: Consider the following smooth simplified continuum model for a one-dimensional granular flow with smooth non-characteristic initial data:

$$\begin{aligned} u_t + u\, u_x &= 1, \\ \rho_t + u\rho_x &= -u_x \rho, \end{aligned}$$

for $x, t \geq 0$, with initial conditions

$$u(x,0) = -x,\ \rho(x,0) = 1.$$

For the method of characteristics (cf. [31, 40]), one solves

$$dt = \frac{dx}{u} = \frac{du}{1} = \frac{d\rho}{-u_x \rho}$$

subject to the initial conditions. A bit of straightforward computation leads to the local (in time) solution

$$u(x,t) = \frac{2(t-x) - t^2}{2(1-t)},\ \rho(x,t) = \frac{1}{1-t},$$

which clearly develops a shock at $t = 1$, and shows that the local (in time solution) cannot be continued beyond $t = 1$. Note that the solution here is such that the density is unbounded, which is certainly not physically consistent with a material granular column having some inherent rigidity.

The following example of a simplified system is a globally well-posed:

Example B: The initial value problem this time is as follows:

$$u_t + u\, u_x = -u,$$

$$\rho_t + u\rho_x = -u_x \rho,$$

for $x, t \geq 0$, with initial data

$$u(x,0) = 1,\ \rho(x,0) = \psi(x),$$

where ψ and ψ_x are continuous and bounded on $\mathbb{R}$. The characteristic equations are

$$dt = \frac{dx}{u} = \frac{du}{-u} = \frac{d\rho}{-u_x \rho}$$

subject to the specified initial conditions, which yield the unique global solution

$$u(x,t) = e^{-t},\ \rho(x,t) = \psi\left(x + e^{-t} - 1\right).$$

Observe that in this case the density is globally bounded as one would expect for a physically realistic solution.

The above examples indicate that in order to guarantee global well-posedness for the initial value problem (3.18) - (3.19), it is going to be necessary to have hypotheses that includes some degree of boundedness on the density to insure that the characteristic flow-generated integral submanifold of the prescribed initial data submanifold comprises a sufficiently smooth graph of the domain of the system. And it shall be shown that such a density bound is actually a key ingredient in the proof.

3.3.2 Local Well-posedness of the Model

The analysis begins with a local well-posedness result that is stated and proved in what follows. First, it is useful and in fact almost necessary to introduce some fairly standard notation from functional analysis. Let $F : S \to \mathbb{R}^m$ be a map from a (Lebesgue measurable) subset S of $\mathbb{R}^n$ into $\mathbb{R}^m$. The following definitions are often used:

$$C\left(S, \mathbb{R}^m\right) := \{F : F \text{ is a continuous on } s\},$$
$$C_B\left(S, \mathbb{R}^m\right) := \{F : F \ \in C\left(S, \mathbb{R}^m\right) \text{ and } \sup\{|F(x)| : x \in S\} < \infty\},$$

where $|\cdot|$ is the appropriate Euclidean norm,

$$C^{(k)}\left(S, \mathbb{R}^m\right) := \{F : F \text{ and all derivatives } D^\alpha F, 1 \leq |\alpha| \leq k, \text{ are continuous on } S\},$$
$$C_B^{(k)}\left(S, \mathbb{R}^m\right) := \{F : F \text{ and all derivatives } D^\alpha F, 1 \leq |\alpha| \leq k, \text{ belong to } C_B\left(S, \mathbb{R}^m\right)\}.$$

Here D^α is the usual multi-index notation for higher order derivatives, namely $\alpha = (\alpha_1, \ldots, \alpha_n)$ is an n-tuple of nonnegative integers with $|\alpha| := \alpha_1 + \cdots + \alpha_n$ and

$D^\alpha F := \partial_{x_1}^{\alpha_1} \cdots \partial_{x_n}^{\alpha_n} F$. Also among the definitions to be used are the following:

$$C^\infty(S, \mathbb{R}^m) := \{F : F \text{ and all derivatives } D^\alpha F, 1 \leq |\alpha|, \text{ are continuous on } S\},$$

$$C_B^\infty(S, \mathbb{R}^m) := \{F : F \text{ and all derivatives } D^\alpha F, 1 \leq |\alpha|, \text{ belong to } C_B(S, \mathbb{R}^m)\}.$$

Supremum norms can be defined on some of the above spaces. These have the form

$$\|F\|_* := \sup\{|F(x)| : x \in S\}$$

and for $k > 0$,

$$\|F\|_{*,k} := \sup\{\sum\nolimits_{0 \leq |\alpha| \leq k} |D^\alpha F(x)| : x \in S\},$$
$$\|F\|_{*,\infty} := \sup\{\sum\nolimits_{0 \leq |\alpha|} 2^{-|\alpha|} |D^\alpha F(x)| : x \in S\}.$$

It should be noted that $C_B(S, \mathbb{R}^m)$ equipped with $\|\cdot\|_*$, $C_B^{(k)}(S, \mathbb{R}^m)$ equipped with $\|\cdot\|_{*,k}$ and $C_B^\infty(S, \mathbb{R}^m)$ equipped with $\|F\|_{*,\infty}$ are all Banach spaces.

There are also several handy spaces, called Sobolev spaces, that are defined in terms of integrals; namely

$$H^{k,p}(S, \mathbb{R}^m) := \left\{ \begin{array}{c} F : F \text{ is in the completion of } C^{(k)}(S, \mathbb{R}^m) \text{ with respect to} \\ \|F\|_{k,p} := \left[\int_S \left(\sum\nolimits_{0 \leq |\alpha| \leq k} |D^\alpha F(x)|^p\right) dx\right]^{1/p} (< \infty) \end{array} \right\}$$

for $p \geq 1$, where the integral is the Lebesgue integral in $\mathbb{R}^n$. The spaces $H^{k,p}(S, \mathbb{R}^m)$ equipped with $\|\cdot\|_{k,p}$ are all Banach spaces and $H^{k,2}(S, \mathbb{R}^m)$ is, in fact, a Hilbert space. These Banach spaces defined in terms of integrals actually can be identified with the first series of spaces defined in terms of the behavior of derivatives owing to a series of embedding theorems obtained by by Sobolev, Kondrachov and Rellich (see [1]). These embedding theorems are extremely useful in passing from weak solutions to classical solutions in the analysis of partial differential equations, as illustrated in [31, 47].

The local well-posedness can best be demonstrated by recasting (3.18) in the form

$$\boldsymbol{u}_t + \langle \boldsymbol{u}, \nabla \rangle \, \boldsymbol{u} = \boldsymbol{F}\left(\boldsymbol{x}, t, \boldsymbol{u}, \rho; \mu\right), \tag{3.20}$$

$$\rho_t + \langle \boldsymbol{u}, \nabla \rangle \, \rho = -\rho \mathrm{tr} \boldsymbol{u}_{\boldsymbol{x}}, \tag{3.21}$$

where

$$\boldsymbol{F}\left(\boldsymbol{x}, t, \boldsymbol{u}, \rho; \mu\right) := \boldsymbol{\alpha}(\boldsymbol{x}, t; \mu) + \int_{B_r(x)} \rho(\boldsymbol{y}, t) \boldsymbol{\Theta}(\boldsymbol{x}, \boldsymbol{y}, \boldsymbol{u}(\boldsymbol{x}, t), \boldsymbol{u}(\boldsymbol{y}, t)) d\boldsymbol{y}.$$

Then it follows from the method of characteristics (see, e.g. [31]) that local solutions can be swept out in (x, t, u, ρ)-space by the system of ODEs

$$\frac{dt}{ds} = 1, \ \frac{d\boldsymbol{x}}{ds} = \boldsymbol{u}, \ \frac{d\boldsymbol{u}}{ds} = \boldsymbol{F}\left(\boldsymbol{x}, t, \boldsymbol{u}, \rho; \mu\right), \ \frac{d\rho}{ds} = -\rho \mathrm{tr} \boldsymbol{u}_{\boldsymbol{x}}, \tag{3.22}$$

subject to the in initial data

$$t(0) = t_0 = 0, \ \boldsymbol{x}(0) = \boldsymbol{x}_0 = \boldsymbol{\xi}, \ \boldsymbol{u}(0) = \boldsymbol{u}_0 = \boldsymbol{u}_0(\boldsymbol{\xi}), \ \rho(0) = \rho_0 = \rho_0(\boldsymbol{\xi}). \tag{3.23}$$

Integration of (3.22) subject to (3.23) yields

$$\boldsymbol{x}\left(\boldsymbol{\xi}, t\right) = \boldsymbol{\xi} + \int_0^t \boldsymbol{u}\left(\boldsymbol{x}(\boldsymbol{\xi}, \tau), \tau\right) d\tau, \tag{3.24}$$

$$\boldsymbol{u}\left(\boldsymbol{\xi}, t\right) = \boldsymbol{u}_0(\boldsymbol{\xi}) + \int_0^t \boldsymbol{F}\left(\boldsymbol{x}, t, \boldsymbol{u}, \rho; \mu\right) d\tau, \tag{3.25}$$

$$\rho\left(\xi, t\right) = \rho_0(\boldsymbol{\xi}) \exp\left[-\int_0^t \left(\sum\nolimits_{k=1}^{n} \partial_{x_k} u_k\left(\boldsymbol{\xi}, t\right)\right) d\tau\right]. \tag{3.26}$$

It is interesting from a physical perspective to note that if the initial density is nonnegative on on the spatial domain Ω, then it follows from (3.26) that the density remains nonnegative for all time, which is physically consistent.

As the right-hand side of equations (3.24)-(3.26) also depend on $\boldsymbol{u}_{\boldsymbol{x}}$, it is necessary to add a consistent time-integrated form of a differential equation for this

extra variable in to make a complete system of ODEs. It follows from standard results on ODEs, such as can be found in [13, 20], that if the original system is sufficiently continuously differentiable, this equation must have the form

$$\boldsymbol{u}_{\boldsymbol{x}}(\xi,t) = \partial_{\boldsymbol{x}}\boldsymbol{u}_0(\boldsymbol{\xi}) + \int_0^t \partial_{\boldsymbol{x}}\boldsymbol{F}\left(\boldsymbol{x},t,\boldsymbol{u},\rho;\mu\right)d\tau,$$

so the equations to solve in order to sweep out solutions of (3.18)-(3.19) is the system of $n(n+2)$ equations

$$\boldsymbol{x}\left(\boldsymbol{\xi},t\right) = \boldsymbol{\xi} + \int_0^t \boldsymbol{u}\left(\boldsymbol{x}(\boldsymbol{\xi},\tau),\tau\right)d\tau, \tag{3.27}$$

$$\boldsymbol{u}\left(\boldsymbol{\xi},t\right) = \boldsymbol{u}_0(\boldsymbol{\xi}) + \int_0^t \boldsymbol{F}\left(\boldsymbol{x},t,\boldsymbol{u},\rho;\mu\right)d\tau, \tag{3.28}$$

$$\boldsymbol{u}_{\boldsymbol{x}}(\xi,t) = \partial_{\boldsymbol{x}}\boldsymbol{u}_0(\boldsymbol{\xi}) + \int_0^t \partial_{\boldsymbol{x}}\boldsymbol{F}\left(\boldsymbol{x},t,\boldsymbol{u},\boldsymbol{u}_{\boldsymbol{x}};\mu\right)d\tau, \tag{3.29}$$

in which the formula in (3.26) has been substituted for ρ in the last of the above equations. Of course, these equations are solutions of the system of ODEs from which they are derived subject to the initial conditions

$$\boldsymbol{x}\left(\boldsymbol{\xi},0\right) = \boldsymbol{\xi},\ \boldsymbol{u}\left(\boldsymbol{\xi},0\right) = \boldsymbol{u}_0(\boldsymbol{\xi}),\ \boldsymbol{u}_{\boldsymbol{x}}(\xi,0) = \partial_{\boldsymbol{x}}\boldsymbol{u}_0(\boldsymbol{\xi}). \tag{3.30}$$

It often convenient to represent all of the systems above in a more concise form by first defining $\boldsymbol{w} := (\boldsymbol{x},\boldsymbol{u},\boldsymbol{u}_{\boldsymbol{x}}) \in \mathbb{R}^{n(n+2)}$ and then recasting the system of characteristic-like ODEs (3.22) as

$$\dot{\boldsymbol{w}} = \boldsymbol{G}\left(t,\boldsymbol{w};\mu\right), \tag{3.31}$$

subject to the initial condition

$$\boldsymbol{w}(0) := \boldsymbol{w}_0 = \left(\boldsymbol{\xi},\boldsymbol{u}_0(\boldsymbol{\xi}),\partial_{\boldsymbol{x}}\boldsymbol{u}_0(\boldsymbol{\xi})\right). \tag{3.32}$$

Then integration of (3.31) subject to (3.32) yields the following concise form of (3.27)-(3.30):

$$\boldsymbol{w}(\boldsymbol{\xi},t)=\boldsymbol{w}_0\left(\boldsymbol{\xi}\right)+\int_0^t\boldsymbol{G}\left(\tau,\boldsymbol{w};\mu\right)d\tau. \tag{3.33}$$

The first well-posedness result that follows is local in both space and time.

Lemma 3.1. *Let* $\boldsymbol{\xi}_{\#}=\boldsymbol{x}_{\#}$ *be a specified point in* $\mathbb{R}^n$, $\boldsymbol{w}_0\in C^{(k+1)}\left(\mathbb{R}^n,\mathbb{R}^{n(n+2)}\right)$ *and*

$$G\in C^{(k+1)}\left([0,\infty)\times\mathbb{R}^{n(n+2)}\times U,\mathbb{R}^{n(n+2)}\right),$$

where $k\geq 2$ *and* U *is an open neighborhood in a Euclidean parameter space. Then there exist* $r_{\#},t_{\#}>0$ *such that* (3.18)-(3.19) *has a unique* $C^{(2)}$ *solution in all of its variables and parameters on* $[0,t_{\#})\times B_{r_{\#}}\left(\boldsymbol{\xi}_{\#}\right)\times V$, *where* V *is a nonempty open neighborhood of* U.

Proof: The differentiability hypotheses and basic theorems on solutions of ODEs (such as in [13, 20]) guarantee that (3.33) has a unique, locally $C^{(k)}$ solution in all of its variables and parameters as specified above, except that $t_{\#}$ and $r_{\#}$ are replaced by positive numbers t_1 and r_1, respectively. However, it remains to translate this to solutions of (3.18)-(3.19). This requires the unique smooth solvabiliy of (3.27), recast as

$$X=X\left(\boldsymbol{\xi},\boldsymbol{x},t\right):=\boldsymbol{\xi}-\boldsymbol{x}+\int_0^t\boldsymbol{u}\left(\boldsymbol{x}(\boldsymbol{\xi},\tau),\tau\right)d\tau=0, \tag{3.34}$$

for ξ as a function of (x,t), where it is useful to note that $\boldsymbol{u}$ is actually a $C^{(k+1)}$ function owing to the details of the ODE existence, uniqueness and differentiability theorems invoked above. Then, a simple computation yields

$$\partial_{\boldsymbol{\xi}}X=\mathbf{1}+\int_0^t\boldsymbol{u}_x\left(\boldsymbol{x}(\boldsymbol{\xi},\tau),\tau\right)\boldsymbol{x}_{\boldsymbol{\xi}}(\boldsymbol{\xi},\tau)d\tau, \tag{3.35}$$

where $\mathbf{1}$ is the identity map on $\mathbb{R}^n$. Hence, $\partial_{\boldsymbol{\xi}} X(\boldsymbol{\xi}, \boldsymbol{x}, 0) = \mathbf{1}$ for all $x \in \Omega$, which in virtue of the implicit function theorem implies that (3.34) has a unique continuous solution of the form

$$\boldsymbol{\xi} = \boldsymbol{\Phi}(\boldsymbol{x}, t), \tag{3.36}$$

which actually belongs to $C^{(k+1)}\left([0, t_2) \times B_{r_2}\left(\boldsymbol{\xi}_{\#}\right)\right)$ for some $r_2, t_2 > 0$.

Now define $t_{\#} := \min\{t_1, t_2\}$ and $r_{\#} := \min\{r_1, r_2\}$. Then it follows from the derivation of (3.33) as the integral form of the characteristic ODEs that sweep out the solution of the initial value problem (3.18)-(3.19), that substitution of (3.36) in (3.25) and (3.26) leads to

$$\begin{aligned}
&\boldsymbol{u}(\boldsymbol{x}, t) = \boldsymbol{u}(\boldsymbol{x}, t; \mu) := \boldsymbol{u}(\boldsymbol{\Phi}(\boldsymbol{x}, t), t), \\
&\rho(\boldsymbol{x}, t) = \rho(\boldsymbol{x}, t; \mu) := \rho_0(\boldsymbol{\Phi}(\boldsymbol{x}, t)) \exp\left[-\int_0^t \operatorname{tr} \boldsymbol{u}_{\boldsymbol{x}}(\boldsymbol{\Phi}(\boldsymbol{x}, \tau), \tau)\, d\tau\right],
\end{aligned} \tag{3.37}$$

which is a solution of (3.18)-(3.19) in $C^{(k)}\left([0, t_{\#}) \times B_{r_{\#}}\left(\boldsymbol{\xi}_{\#}\right) \times V\right)$. Conversely, any $C^{(1)}$ solutions of (3.18)-(3.19) must be swept by solutions of (3.33), which guarantees the uniqueness. Thus, the proof is complete. □

It is easy to see that Lemma 3.1 has an analog - proved by making some simple obvious adjustments in the argument above - for positive initial points $t_0 > 0$ if the initial data is just as smooth as it is at $t_0 = 0$; namely the following result.

Lemma 3.2. *Let $\boldsymbol{\xi}_{\#}$ be a specified point in $\mathbb{R}^n, \boldsymbol{w}_0(\cdot, t_0) \in C^{(k+1)}\left(\mathbb{R}^n, \mathbb{R}^{n(n+2)}\right)$, with $t_0 > 0$,*

$$G \in C^{(k+1)}\left([0, \infty) \times \mathbb{R}^{n(n+2)} \times U, \mathbb{R}^{n(n+2)}\right),$$

where $k \geq 2$ and U is an open neighborhood in a Euclidean parameter space. Then there exist $r_{\#}, a > 0$ such that (3.18)-(3.19) has a unique $C^{(2)}$ solution in all of its variables and parameters on $[t_0 - a, t_0 + a] \times B_{r_{\#}}\left(\boldsymbol{\xi}_{\#}\right) \times V$, where $0 < a < t_0$ and V is a nonempty open neighborhood of U.

Note that if Ω were compact, $\Omega \times \{t_0\}$ could be covered by finitely many open balls of the type described in the above lemmas, which would then directly lead to the local in time only results that follow.

Lemma 3.3. *Let Ω be compact, $\boldsymbol{\xi}_{\#} = \boldsymbol{x}_{\#}$ be a specified point in $\mathbb{R}^n$, $\boldsymbol{w}_0 \in C^{(k+1)}\left(\mathbb{R}^n, \mathbb{R}^{n(n+2)}\right)$ and*

$$G \in C^{(k+1)}\left([0,\infty) \times \mathbb{R}^{n(n+2)} \times U, \mathbb{R}^{n(n+2)}\right),$$

where $k \geq 2$ and U is an open neighborhood in a Euclidean parameter space. Then there exist $t_{\#} > 0$ such that (3.18)-(3.19) has a unique $C^{(2)}$ solution in all of its variables and parameters on $[0, t_{\#}) \times \Omega \times V$, where V is a nonempty open neighborhood of U.

Lemma 3.4. *Let Ω be compact, $\boldsymbol{\xi}_{\#}$ be a specified point in $\mathbb{R}^n, \boldsymbol{w}_0(\cdot, t_0) \in C^{(k+1)}\left(\mathbb{R}^n, \mathbb{R}^{n(n+2)}\right)$, with $t_0 > 0$,*

$$G \in C^{(k+1)}\left([0,\infty) \times \mathbb{R}^{n(n+2)} \times U, \mathbb{R}^{n(n+2)}\right),$$

where $k \geq 2$ and U is an open neighborhood in a Euclidean parameter space. Then there exist $t_{\#} > 0$ such that (3.18)-(3.19) has a unique $C^{(2)}$ solution in all of its variables and parameters on $[t_0 - a, t_0 + a] \times \Omega \times V$, where $0 < a < t_0$ and V is a nonempty open neighborhood of U.

If Ω is not compact, it is necessary to have either global *a priori* estimates of some kind or uniform global bounds to obtain local in time only well-posedness, such as in the following theorem.

Theorem 3.1. *(i) Suppose that in addition to the hypotheses of Lemma 3.1, the $r_{\#}, t_{\#} > 0$ apply uniformly for all $\boldsymbol{x}_{\#} \in \Omega$ and there exists a $b > 0$ such that $\sup\left\{\|u(\cdot,t)\|_{*,1} : 0 \leq t \leq b\right\} < \infty$.* Then there is a $t_* > 0$ *such that* (3.18)-(3.19) *has*

a unique $C^{(2)}$ solution in all of its variables and parameters on $[0, t_*) \times \Omega \times V$, where V is a nonempty open neighborhood of U.

(ii) Analogously, suppose that in addition to the hypotheses of Lemma 3.2, the $r_\#, t_\# > 0$ apply uniformly for all $\boldsymbol{x}_\# \in \Omega$ and there exists a $a > 0$ such that $\sup\left\{\|u(\cdot, t_0)\|_{*,1} : t_0 - a \le t \le t_0 + a\right\} < \infty$. Then there is a positive $a_* \le a$ such that (3.18)-(3.19) *has a unique $C^{(2)}$ solution in all of its variables and parameters on $[t_0 - a_*, t_0 + a_*] \times \Omega \times V$, where V is a nonempty open neighborhood of U.*

Proof. It suffices to prove the contention (i), since the argument for (ii) requires only straightforward adjustments of the kind used to infer Lemma 3.2 from Lemma 3.1. From the proof of Lemma 3.1 and the hypotheses of the theorem, it follows that (3.33) has unique $C^{(k)}$ solution in all of its variables and parameters on $[0, t_\#) \times \Omega \times V$, where V is a nonempty open neighborhood of U. Consequently, it follows from the proof of Lemma 3.1 that it remains only to show that there is a $0 < t_* \le t_\#$ such that (3.34) is uniquely smoothly solvable as $\boldsymbol{\xi} = \boldsymbol{\Phi}(\boldsymbol{x}, t)$ on $\Omega \times [0, t_*)$. Toward this end, consider the equation obtained by differentiating (3.27) with respect to $\boldsymbol{\xi}$, namely

$$\boldsymbol{x}_{\boldsymbol{\xi}}(\boldsymbol{\xi}, t) = \mathbf{1} + \int_0^t \boldsymbol{u}_x\left(\boldsymbol{x}(\boldsymbol{\xi}, \tau), \tau\right) \boldsymbol{x}_{\boldsymbol{\xi}}(\boldsymbol{\xi}, \tau) d\tau. \tag{3.38}$$

It follows from the assumption concerning $\|u(\cdot, t)\|_{*,1}$ that there is an $M > 0$ such that

$$\|\boldsymbol{x}_{\boldsymbol{\xi}}(\boldsymbol{\xi}, t)\| \le 1 + M \int_0^t \|\boldsymbol{x}_{\boldsymbol{\xi}}(\boldsymbol{\xi}, \tau)\| \, d\tau \tag{3.39}$$

for all $(\boldsymbol{\xi}, t) \in \Omega \times [0, b]$. Therefore, it follows from Gronwall's inequality (see, e.g. [20]) that

$$\|\boldsymbol{x}_{\boldsymbol{\xi}}(\boldsymbol{\xi}, t)\| \le e^{Mt}$$

on $\Omega \times [0, b]$, which implies that

$$\left\| \int_0^t \boldsymbol{u}_x\left(\boldsymbol{x}(\boldsymbol{\xi}, \tau), \tau\right) \boldsymbol{x}_{\boldsymbol{\xi}}(\boldsymbol{\xi}, \tau) d\tau \right\| \le \int_0^t M e^{M\tau} d\tau = e^{Mt} - 1, \tag{3.40}$$

so it follows from (3.38) that there exists a $0 < t_* \leq t_\#$ such that

$$\|\boldsymbol{x}_{\boldsymbol{\xi}}(\boldsymbol{\xi}, t) - \mathbf{1}\| \leq 1/2$$

for all $(\boldsymbol{\xi}, t) \in \Omega \times [0, b]$. But this implies that (3.34) is uniquely, smoothly solvable in the form (3.36), which completes the proof. $\square$

3.3.3 Global Well-posedness

All the tools have now been assembled for the main global well-posedness theorem, which takes its cue from Theorem 3.1. The first result establishes semi-global well-posedness for the integral equation (3.33).

Lemma 3.5. *Suppose that* (3.33) *satisfies the following properties*:

(i) *The initial data* $\boldsymbol{w}_0 \in C_B^{(m)}(\Omega)$ for every $m \in \mathbb{N}$.

(ii) $G \in C_B^{(k+1)}\left([0, T) \times \mathbb{R}^{n(n+2)} \times U, \mathbb{R}^{n(n+2)}\right)$ for every $T > 0$, where $k \geq 2$.

Then there exists a $t_\# > 0$ *such that* (3.33) *has unique* $C^{(k)}$ *solution in all of its variables and parameters on* $[0, t_\#) \times \Omega \times V$, *where* V *is a nonempty open neighborhood of* U. *Moreover, if*

(iii) The initial function $\boldsymbol{w}_0(\cdot, t_0) \in C^{(k+1)}\left(\mathbb{R}^n, \mathbb{R}^{n(n+2)}\right)$, *with* $t_0 > 0$,

there exists an $a > 0$ *such that* (3.33) *has unique* $C^{(k)}$ *solution in all of its variables and parameters on* $[0, \infty) \cap [t_0 - a, t_0 + a] \times \Omega \times V$.

Proof. The proof follows directly from Theorem 3.1 once the uniform interval of existence can be established. This is a result primarily due to the way in which the local existence and uniqueness of the solutions of (3.33) is established using Banach's fixed point theorem. In particular, choose any $t_0 \geq 0$ and set $T = t_0 + 1$. Then (ii)

and (iii) imply that there exists an $M > 0$ such that for any two $C_B^{(k+1)}$ solutions $\boldsymbol{w}$ and $\hat{\boldsymbol{w}}$ of (3.33) in the t interval $R(t_0) := [0,\infty) \cap [t_0 - (1/2), t_0 + (1/2)]$ satisfy

$$\|\hat{\boldsymbol{w}} - \boldsymbol{w}\|_{*,k+1} \leq M \left| \int_{t_0}^{t} \|\hat{\boldsymbol{w}} - \boldsymbol{w}\|_{*,k+1} \, d\tau \right| = M \, |t - t_0| \, \|\hat{\boldsymbol{w}} - \boldsymbol{w}\|_{*,k+1} \, . \tag{3.41}$$

Accordingly, the right-hand side of (3.33) is a contraction mapping whenever $|t - t_0| < 1/M$, and this is uniformly valid on $\Omega \times \{t_0\}$. Hence, it follows from the contraction mapping theorem that the interval of existence of any (unique) $C_B^{(k+1)}$ solution of (3.33) is at least $[0,\infty) \cap [t_0 - a_0, t_0 + a_0]$ for every $(\boldsymbol{x}, t_0) \in \Omega \times \{t_0\}$. Moreover, $\|\boldsymbol{u}_x\|$ is bounded on $[0,\infty) \cap [t_0 - a_0, t_0 + a_0] \times \Omega$, so it follows that just as in (3.38)-(3.40) of the proof of Theorem 3.1, it can be established that (3.34) with $t = t_0$ has a unique $C_B^{(k+1)}$ solution of the form $\boldsymbol{\xi} = \boldsymbol{\Phi}(\boldsymbol{x}, t)$ on $\Omega \times [0,\infty) \cap [t_0 - a, t_0 + a]$ for some $0 < a \leq a_0$. Therefore, Theorem 3.1 implies the desired result, and the proof is complete. $\square$

Finally the global well-posedness proof is now easily within reach.

Theorem 3.2. *Suppose that the following properties obtain*:

(I) *The function* α *defined after (3.21) is in* $C_B^{(k+1)}\left([0,\infty) \times \mathbb{R}^{n(n+2)}) \times U, \mathbb{R}\right)$, *where* $k \geq 2$.

(II) *The integral*
$\int_{B_r(x)} \rho(y,t)\Theta(x,y,u(x,t),u(y,t))dy \in C_B^{(k+1)}\left([0,T) \times \mathbb{R}^{n(n+2)}) \times U, \mathbb{R}^{n(n+2)}\right)$ *for every* $T > 0$, *where* $k \geq 2$.

Then (3.18)-(3.19) *has a unique* $C^{(2)}$ *solution in all of its variables and parameters on* $[0,\infty) \times \Omega \times V$, *where* V *is a nonempty open neighborhood of* U.

Proof. First, note that
$\int_{B_r(x)} \rho(y,t)\Theta(x,y,u(x,t),u(y,t))dy \in C_B^{(k+1)}\left([0,T) \times \mathbb{R}^{n(n+2)}) \times U, \mathbb{R}^{n(n+2)}\right)$ implies

that

$$\partial_{\boldsymbol{x}} \int_{B_r(x)} \rho(y,t)\Theta(x,y,u(x,t),u(y,t))dy \in C_B^{(k)}\left([0,T)\times\mathbb{R}^{n(n+2)})\times U,\mathbb{R}^{n(n+2)}\right).$$

This property, which is a nice illustration of the mediating effects of the integral representation, follows directly from the observation that

$$\partial_{\boldsymbol{x}_k} \int_{B_r(x)} \rho(y,t)\Theta(x,y,u(x,t),u(y,t))dy = \int_{B_r(x)}^{(k)} \rho(y,t)\Theta(x,y,u(x,t),u(y,t))dy + \int_{B_r(x)} \partial_{\boldsymbol{x}_k}[\rho(y,t)\Theta(x,y,u(x,t),u(y,t))]dy, \tag{3.42}$$

where $\int_{B_r(x)}^{(k)}$ denotes the $(n-1)$-dimensional integral over the slice of the ball with the coordinate x_k fixed in the reduced dimensional arguments in the first of the integrals on the right-hand side of the above equation. Consequently, (i) - (iii) of Lemma 3.5 are satisfied.

It still needs to be shown that the solution of (3.18)-(3.19) associated to the uniform solution is global in t. Suppose not, then the intervals of existence $[0,t_m)$ must have a supremum $t_\infty < \infty$, for which there is a sequence $\{t_m\}$ with $t_m \uparrow t_\infty$. In particular, there is an m such $t_\infty - t_m < a$, where a is the uniform bound described in Theorem 3.1. But the local well-posedness shows that the uniqueness together with above local result contradicts the extendability of the solution intervals. Thus, the proof is complete. □

A close examination of the above proofs now reveals that an a priori bound on the density is indeed the key ingredient for global well-posedness of the initial value problem (3.18) - (3.19). In fact, following the steps in the above arguments with special attention to (3.42), it is a straightforward matter to prove the following result involving rather mild, physically realistic assumptions.

Corollary 3.1. Let (3.18) - (3.19) *satisfy the following properties*:

(i) *The external force per unit volume* $\boldsymbol{\alpha} \in C_B^2(\Omega \times [0,T] \times \Pi)$ *for every* $T > 0$, *where* Π *is the parameter space.*

(ii) *The boundary data* $u_0, \rho_0 \in C_B^2(\Omega)$.

(iii) *The interaction kernel* $\boldsymbol{\Theta} \in C_B^2(\Omega \times \mathbb{R}^n \times \mathbb{R}^n)$.

(iv) *The density* $\rho \in C_B^2(\Omega \times [0,T])$ *for every* $T > 0$.

Then the initial value problem has a unique, C^1 *solution on* $\Omega \times [0,\infty)$ *that is continuously dependent on the initial data and the parameter.*

As a concluding remark, preliminary investigations employing Sobolev space techniques and especially the Sobolev–Rellich–Kondrachov embedding theorem (cf. [1, 31]), give strong indications that the hypotheses of Theorem 3.2 can be relaxed and the following result can be proved using a modification of a standard fixed point formulation for hyperbolic systems such as described in [31].

Conjecture. *Suppose that* $\alpha \in C_B^{(k+1)}\left([0,\infty) \times \mathbb{R}^{n(n+2)}) \times U, \mathbb{R}\right) \cap H^{k,2}\left([0,\infty) \times \mathbb{R}^{n(n+2)}\right)$ *and*

$$\int_{B_r(x)} \rho(y,t)\Theta(x,y,u(x,t),u(y,t))dy \in H^{k,2}\left([0,\infty) \times \mathbb{R}^{n(n+2)}) \times U, \mathbb{R}^{n(n+2)}\right)$$

then (3.18)-(3.19) *has a unique global solution (weak) solution in* $H^{k,2}(\Omega \times [0,\infty) \times \Pi)$, *and therefore a classical solution that is* C^1 *in all of its variables and parameters if* k *is sufficiently large.*

CHAPTER 4

A NUMERICAL SCHEME FOR THE BSR EQUATION: IMPLEMENTATION AND COMPARISONS

The analysis of well-posedness of the BSR equation leads itself naturally to a semidiscrete method. A finite difference (central difference) scheme for the space variable and an accurate one-step explicit integration method for time such as the 3^{th} order Runge–Kutta algorithm, preferably with a variable step size capability, is applied.

One wants a local approximation error of at least order two and a guarantee of numerical stability with regard to the time and space step sizes. What is more, it is preferable to have a scheme for which improvement in accuracy are easily made both in time and space. Here Runge-Kutta (R-K) is a good choice since there is a standard family of methods to improve the time accuracy if so desired; and higher order central difference are able to implemented to couple the R-K without much trouble. The accuracy of the implemented numerical scheme is studied in section 5.2.

In what follows, for simplicity, the domain is assumed to do not vary with time, which can always be achieved if the domain varies rigidly with time —simply by using an inertial coordinate system moving with the motion of the configuration.

There are two choices. (a) use (3.7)-(3.9) directly to find the velocity and density fields. The equations are simpler, but finally the velocity field must be integrated to determine the flow of the original continuum configuration of material; or (b) Use just the momentum equation coupled with (3.10)-(3.12), in which case the equations are more complicated, but the motion of the configuration is computed as part of the numerical scheme.

Here only a brief description of the method for Case (a) is provided. It should be noted that the domains of interest might turn out to be semi-infinite, as for example when a beaker of particles is being accumulatively shaken. In such instances, standard methods for reformulating the numerics in a bounded space domain are used. The semidiscrete approach actually integrates the field at fixed space mesh points over time.

By defining

$$\boldsymbol{\omega} : \Omega_T \mapsto \mathbf{R}^{m+1}, \boldsymbol{\omega} = (\boldsymbol{u}, \boldsymbol{\rho})$$

one can rewrite (3.7)–(3.9) as the functional differential equation plus initial condition

$$\frac{d\boldsymbol{\omega}}{dt} = \boldsymbol{F}(\boldsymbol{x}, t, \boldsymbol{\omega}, \boldsymbol{\omega}_{\boldsymbol{x}}) \tag{4.1}$$

$$\boldsymbol{\omega}(\boldsymbol{x}, 0) = (\boldsymbol{u}(\boldsymbol{x}, \mathbf{0}), \rho(\boldsymbol{x}, 0)) := \boldsymbol{w}(\boldsymbol{x}) \tag{4.2}$$

For simplicity, (4.1)-(4.2) will be considered only for planar space domains. Letting (x_i, y_j) denote the vertices of the space mesh for the domain in $\mathbf{R}^2$, (4.1)-(4.2) is discretized as the system of ODEs

$$\frac{d\boldsymbol{w}}{dt} = \boldsymbol{F}(x_i, y_j, t, \boldsymbol{w}_{ij}\delta\boldsymbol{w}_{ij}), \tag{4.3}$$

$$\boldsymbol{w}_{ij}(0) = \boldsymbol{w}_{ij},$$

where δ denotes an approximation to the partial derivatives of $\boldsymbol{w}$ at the vertex points. This is solved by say, the improved Euler or 4^{th} order Runge–Kutta method, to obtain an approximation to the velocity components and the density at the mesh points. Applying the integration method with respect to t, one obtains a sequence of space-time approximations at all of the mesh points:

$$\{\boldsymbol{w}_{ijk}(x_i, y_j, t_k)\} \tag{4.4}$$

If a modified Euler solver is used to solve (4.3), a quadratic error is obtained in terms of time steps. If a 4^{th} order Runge–Kutta solver is used, then 4^{th} order error estimates will be gotten in time.

The semidiscrete method as described has satisfactory time-domain local truncation errors. However, one needs to be careful about the space derivatives of the density or the velocity in the actual systems, and it does tend to be quite stiff in regions where the partial derivatives are of rather large size and/or vary rapidly in sign. This gives the intuition that some smooth filter should be applied. It will be shown that the moving average technique greatly improves the stability of the numerical scheme (see Chapter 5).

It should be noticed that $\boldsymbol{F}$ in the right hand side of equation (4.3) has an integral term. One can use standard methods to perform this integration quite accurately, but special care must be taken at the boundaries of the computational domain.

One of the main goals is to be able to deal with potential computational instabilities automatically, which must be linked to an inherent ability to monitor the partial derivative approximations.

Our approach to this investigation is three-pronged, comprising principally dissipative particle dynamics simulations, comparisons with physical experiments, and predictions via the derived BSR model.

In the next section, the physical system and important parameters are described, and a detailed explanation of the simulation methodology employed is given in later sections.

4.1 Introduction to 1D Tapping System

As a first step in understanding the more complex, three-dimensional granular container vibration problem, this section presents the findings of our investigations

of a seemingly much simpler system − a one-dimensional tapping column. The 1D tapping problem is also the starting point/(proof-of-concept) case for the BSR approach, which is another reason for first applying the numerical scheme to this problem. While it is quite clear that the column can not serve as a paradigm for the complex dynamics in a three-dimensional system, it may provide some important physical insights. One advantage here is that this starting point provides a great opportunity for comparisons with the results obtained from experiments or discrete element simulations [8, 17, 29, 30].

The first step is to set up the problem of a vertical configuration of particles subject to gravity in which the floor is periodically tapped in an impulsive manner. For this it is assumed that the coordinate system is attached to and moving with the floor of the column.

The granular column comprises N uniform spheres with diameter d and mass m having coordinates $y_k(t), (k = 1, 2, \cdots, N)$, where initially $y_k(0) = (2k-1)\frac{d}{2}, k = 1, 2, \cdots, N$, and $y_0(t)$ denotes the position of the supporting floor. Gravity acts in the $-y$ direction. Taps are modeled by prescribing to the floor a half-sine wave pulse of displacement amplitude a and frequency f. The column is subject to gravity . Some details of the impulse-like taps are given in what follows.

$$y_0(t) = \begin{cases} a\sin(\omega t), & 0 \le t \le \dfrac{\pi}{\omega} \\ 0 \quad , & \dfrac{\pi}{\omega} \le t \le T \end{cases} \tag{4.5}$$

Figure 4.1 depicts the system geometry of the column of spheres (diameter d). Figure 4.2 shows the form of the applied tap of the form $y_0(t)$,

The continuum system is now a combination of the momentum equation and a continuity equation represented as

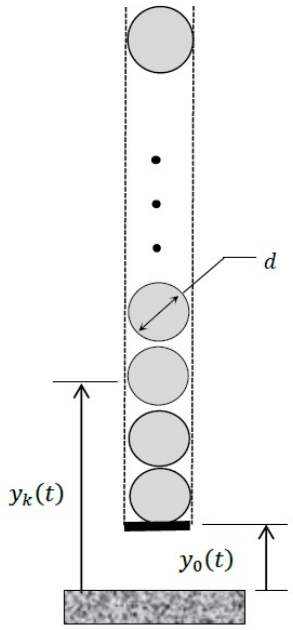

Figure 4.1 Representation of the system geometry of the column of spheres.

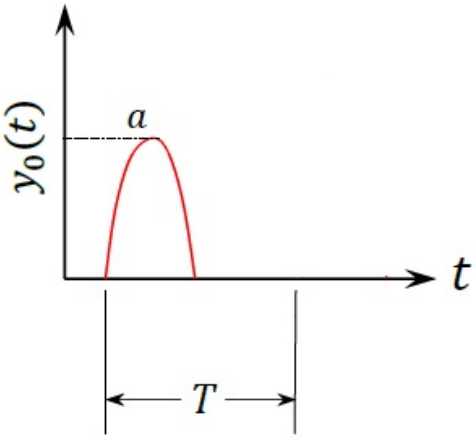

Figure 4.2 The applied tap of the form $y_0(t)$.

$$u_t + uu_y = \frac{K}{m}\int_{-2r}^{2r} \frac{\rho(y+z,t)(2r-|z|)}{m_0}\sigma(z)(1-e\sigma(z[u(y+z)-u(y)]))dz - g + a\omega^2 \sin\omega t \tag{4.6}$$

$$\rho_t + u\rho_y = -u_y\rho \tag{4.7}$$

$$\sigma(s) := \begin{cases} 1, & s > 0 \\ 0, & s = 0 \\ -1, & s < 0 \end{cases} \tag{4.8}$$

where g is the standard acceleration due to gravity, and $a\omega^2 \sin\omega t$ is the inertial force due to the moving coordinate system for the tapping of the column. The constant K is the stiffness coefficient for the interaction kernel chosen, which is the modified (bilinear loading/unloading) Walton–Braun model used in [54] and [55], with a compressive spring constant exceeding the expansive spring constant to capture the energy lost in collision. The $1/mm_0$ in the momentum equation, where m_0 is interpreted as a characteristic mass, corresponds to λ in our general continuum model and is chosen to match the discrete element simulation dynamics. The normalizing and benchmarking value $m_0 = 22kg$ used to determine λ is fixed in the 1D continuum numerical computation. In addition, r represents an average particle radius and m is a standard bead mass $\frac{4}{3}\rho\pi r^3$ from the discrete model. The integral expression on the right-hand side of the momentum equation in (4.6) represents the interaction force per unit mass for the continuum model.

4.2 Review of Numerical Integration and the Finite Difference Scheme

As mentioned earlier, the BSR momentum equation is an integro-PDE, where the integrand is the interaction force kernel. The numerical integration must

be implemented during numerical simulations. A standard five-point numerical integration scheme is used here, which can always be modified to improve the accuracy if so desired.

$$\int_a^b f(x)dx = \frac{b-a}{4}\left(\frac{f(a)}{2} + \sum_{k=1}^{3} f\left(a + k\frac{b-a}{3}\right) + \frac{f(b)}{2}\right) \tag{4.9}$$

In order to deal with the spatial derivative, a finite difference approach is chosen, almost as a matter on necessity. Central differences are chosen to couple the Runge-Kutta method in order to obtain suitable stability, which will be discussed later. Here is a brief review of finite differences.

$$\frac{df}{dx} = \frac{f(x) - f(x-h)}{h} \tag{4.10}$$

$$\frac{df}{dx} = \frac{f(x+h) - f(x)}{h} \tag{4.11}$$

$$\frac{df}{dx} = \frac{f(x+h) - f(x-h)}{2h} \tag{4.12}$$

where equation(4.10)(4.11)(4.12) are the forms corresponding to backward differences, forward difference and central difference, respectively.

Since the domain is a semi-infinite region in space due to the fact that the particles are unconstrained in their movement above the floor, the boundary conditions have to be handled with some care and in particular, an artificial boundary condition must be imposed to make the domain bounded for numerical purposes.

4.3 Implementation of Numerical Schemes

The 1D BSR system is the following,

$$u_t = G(t, \rho, u, u_y) := -uu_y + \lambda \int_{-2r}^{2r} \Theta(\rho)dz - g + a\omega^2 \sin(\omega t) \tag{4.13}$$

$$\rho_t = -(\rho u)_y, \tag{4.14}$$

$$u(y, t = 0) = 0, \tag{4.15}$$

$$\rho(y, t = 0) = \rho_0(y). \tag{4.16}$$

where $\Theta(\rho) := \frac{\rho(y+z,t)(2r-|z|)}{m_0}\sigma(z)(1 - e\sigma(z[u(z+y) - u(y)]))$.

In this section, the RK-3 scheme (check Appendix B for more detail) is coupled with a finite (central) difference scheme to deal with the one-dimensional BSR system. In the equations, i indicates the time mesh and j the space mesh. The velocity and density field (u, ρ) at time $t + \Delta t$ are computed using the following formulas:

$$u_{i+1,j} = u_{i,j} + \frac{1}{6}\left(L^1_{i,j} + 4L^2_{i,j} + L^3_{i,j}\right) \tag{4.17}$$

$$\rho_{i+1,j} = \rho_{i,j} + \frac{1}{6}\left(K^1_{i,j} + 4K^2_{i,j} + K^3_{i,j}\right) \tag{4.18}$$

where

$$L^1_{i,j} = \Delta t \cdot G\left(t, \rho_{i,j}, u_{i,j}, \frac{u_{i,j+1} - u_{i,j-1}}{2\Delta y}\right) \tag{4.19}$$

$$K^1_{i,j} = -\frac{\Delta t}{2\Delta y}\left(u_{i,j+1}\rho_{i,j+1} - u_{i,j-1}\rho_{i,j-1}\right) \tag{4.20}$$

$$\begin{aligned} L^2_{i,j} = \Delta t \cdot G\Bigg\{&(t + \frac{\Delta t}{2}), (\rho_{i,j} + \frac{K^1_{i,j}}{2}), (u_{i,j} + \frac{L^1_{i,j}}{2}), \\ &\frac{(u_{i,j+1} + \frac{L^1_{i,j+1}}{2}) - (u_{i,j-1} + \frac{L^1_{i,j-1}}{2})}{2\Delta y}\Bigg\} \end{aligned} \tag{4.21}$$

$$\begin{aligned} K^2_{i,j} = -\frac{\Delta t}{2\Delta y}\Bigg\{&(u_{i,j+1} + \frac{L^1_{i,j+1}}{2})(\rho_{i,j+1} + \frac{K^1_{i,j+1}}{2}) \\ &- (u_{i,j-1} + \frac{L^1_{i,j-1}}{2})(\rho_{i,j-1} + \frac{K^1_{i,j-1}}{2})\Bigg\} \end{aligned} \tag{4.22}$$

$$L^3_{i,j} = \Delta t \cdot G\Big\{(t+\Delta t), (\rho_{i,j} - K^1_{i,j} + 2K^2_{i,j}), (u_{i,j} - L^1_{i,j} + 2L^2_{i,j}), \\ \frac{(u_{i,j+1} - L^1_{i,j+1} + 2L^2_{i,j+1}) - (u_{i,j-1} - L^1_{i,j-1} + 2L^2_{i,j-1})}{2\Delta y}\Big\} \tag{4.23}$$

$$K^3_{i,j} = -\frac{\Delta t}{2\Delta y}\Big\{(u_{i,j+1} - L^1_{i,j+1} + 2L^2_{i,j+1})(\rho_{i,j+1} - K^1_{i,j+1} + 2K^2_{i,j+1}) \\ - (u_{i,j-1} - L^1_{i,j-1} + 2L^2_{i,j-1})(\rho_{i,j-1} - K^1_{i,j-1} + 2K^2_{i,j-1})\Big\} \tag{4.24}$$

The description of how RK3 and the finite difference scheme are coupled to solve the BSR equation has now been given. Then a 3-mesh (or 5-mesh) moving average at regular intervals is implemented to smooth the data. More precisely, the RK3 scheme combined with central differences is implemented to solve the equation system numerically. In order to ensure that the stability condition is met, a moving average is implemented in space (along y) at every time step Δt, which provides the discrete density and velocity fields used to compute (ρ, u) at the next time instance. The first element of the moving average is obtained by taking the average of the initial three mesh point values of a fixed subset of the data series. Then the subset is modified by "shifting forward".

$$\bar{\rho}_{i,j} = \frac{1}{4}(2\rho_{i,j} + \rho_{i,j+1} + \rho_{i,j-1}) \\ \bar{u}_{i,j} = \frac{1}{4}(2u_{i,j} + u_{i,j+1} + u_{i,j-1})$$

Mathematically, a moving average is a type of convolution and so it can be viewed as an example of a low-pass filter used in signal processing. When used with non-time series data, a moving average filters higher frequency components without any specific connection to time. Viewed simplistically it can be regarded as smoothing

the data. The moving average technique preserves second order accuracy for the overall scheme and improves the stability, which will be shown in Chapter 5.

In the following, a discussion of many other supplementary details involved in implementing the scheme is presented. In the interest of clarity, these issues are explained and illustrated by introducing a simplified version of the 1D tapping system in which the interaction force term is taken to be a constant.

$$u_t + uu_x = \sin(t) - g + \lambda \int \rho(x) \tag{4.25}$$

$$\rho_t + (u\rho)_x = 0 \tag{4.26}$$

$$\begin{aligned} u(x, t = 0) &= 0, \\ \rho(x, t = 0) &= \rho_0(x) \end{aligned} \tag{4.27}$$

where $\rho_0(x)$ is the initial density.

By moving all the terms but the time derivative to the right, the equations (4.25) (4.26) can be rewritten as:

$$u_t = -uu_x + \sin(t) - g + \lambda \int \rho(x) \tag{4.28}$$

$$\rho_t = -(u\rho)_x; \tag{4.29}$$

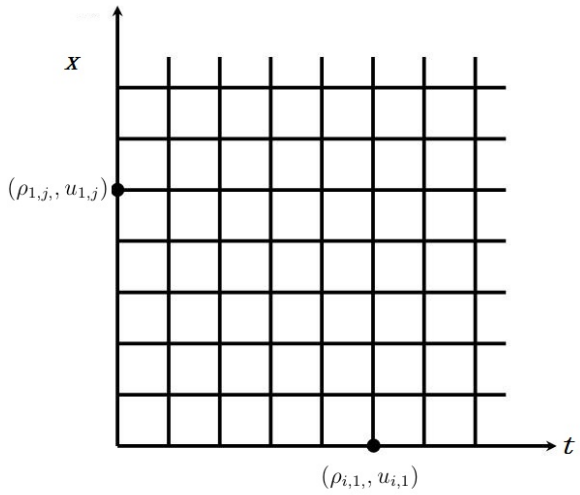

Figure 4.3 Equally spaced numerical grids for both temporal and spatial mesh.

As it is showed earlier, the time derivative are realized by the R-K method. Now the focus is on implementing the central differences for the space derivatives. Here, i is still used for the time mesh and j for the space mesh.

For the intermediate space mesh j, the standard central difference will be implemented to both the momentum and continuity equation as mentioned earlier in this section. While at the boundary, simple boundary and numerical boundary conditions are carefully applied to test the effectiveness of the model, due to the reason that there is no proper boundary integral method or boundary element method in hand to deal with the novel BSR system. For example,

$$\rho_{i+1,1} = \frac{1}{2}(\rho_{i,1} + \rho_{i,2})$$

$$\rho_{i+1,N} = 0$$

$$u_{i+1,N} = u_{i+1,N-1} \tag{4.30}$$

and $u_{i,1}$ will be the velocity corresponding to the floor.

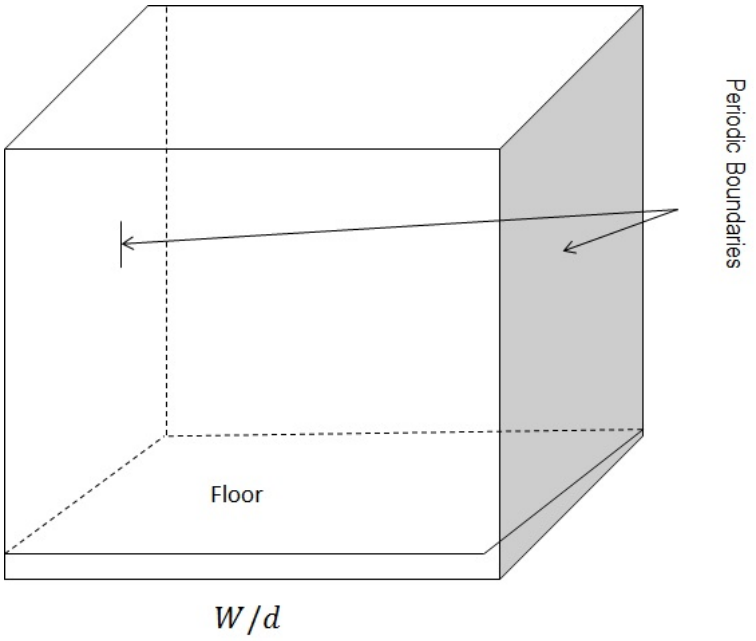

Figure 4.4 Periodic boundaries in (x, z) in 3D geometry.

For $j = N$, this computation is not done using central differences. It should be noted that such boundaries can be identified a priori using simple energy calculations. This is a plausible and physically realistic way of dealing with the semi-infinite domain. It shall be assumed that above the motion of the material column (for which we can find an upper bound) the density is just the constant air density. Clearly, periodic numerical boundary conditions in space domain are not applicable for this problem. These boundary conditions and some of their variant are tested and fit the numerical experiments well, and it should be realized that numerical periodic boundary conditions will come in handy for some horizontal dimensions when the model and numerics are extended to three-dimensional space (Figure 4.4).

4.4 Some Simulation Comparisons

Once the density and velocity fields are approximated using the numerical scheme, the basic information is available to compute the trajectories of individual points in the particle column by (numerically) integrating the velocity field over time. There

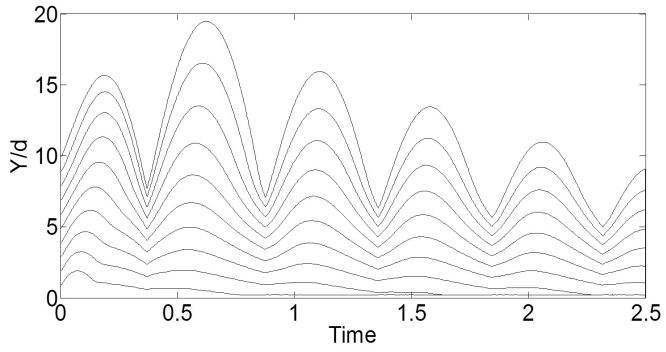

Figure 4.5 Particle trajectories for tapping of ten particle stacks.

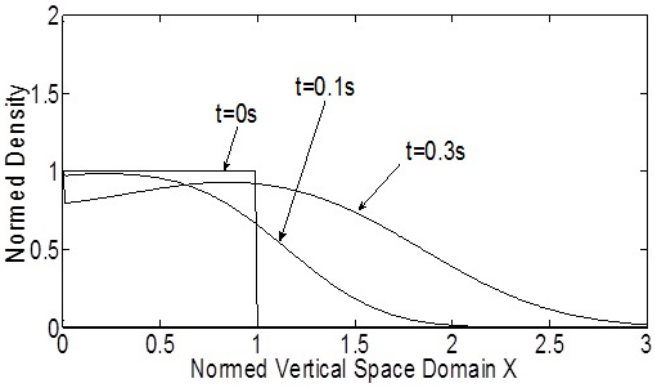

Figure 4.6 Normed density field in normed vertical space at different time.

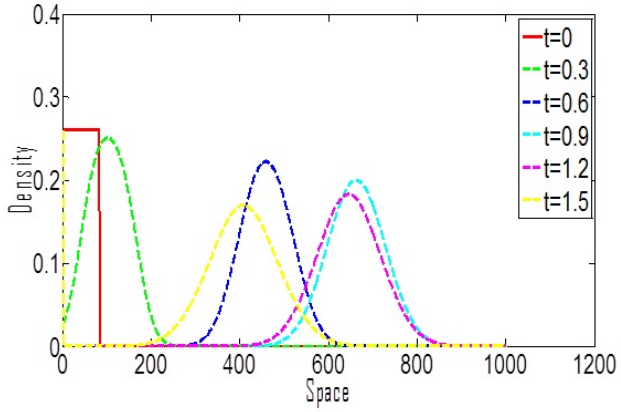

Figure 4.7 Density wave due to a stronger tapping in the first flight time.

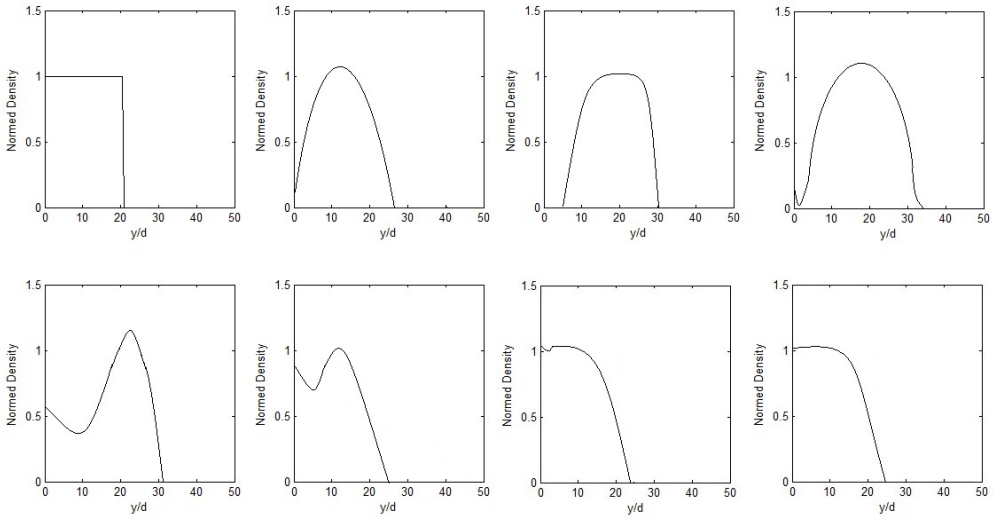

Figure 4.8 Denisty plots at various times due to a single tap of $a = 0.75d$ and $f = 10Hz$. $t = 0.4, 0.5, 0.55, 0.60, 0.65, 0.70, 0.75, 0.80$ respectively.

are several ways of doing so. In the following Euler integration, as an example, will be implemented. Assuming one particle position evolution (trajectory) starting from position P_0, then the the particle position at the next time step is computed as $P_1 = P_0 + u(P_0)dt$. If P_0 is on the mesh grids of the computation domain of the semi-discrete scheme, $u(P_0)$ is ready to use from the data of velocity field. If P_0 is not on the mesh grids, one can apply linear interpolation to get $u(P_0)$, by using the nearby space mesh grid to $y = P_0$. Higher accuracy could be achieved by using advanced time integration and interpolation methods. Figure 4.5 shows one of the numerical experiments on a stack of ten relatively elastic particles with their trajectories due to tapping. Figure 4.6 and figure 4.7 show some density wave results. Figure 4.6 shows the normed density field curve versus the normalized vertical space at $t = 0$, $t = 0.1$ and $t = 0.3$. Figure 4.7 shows the density curve evolution due to a much stronger tap in which the density can be very small near the contact floor due to separation of particle column during flight time around two seconds.

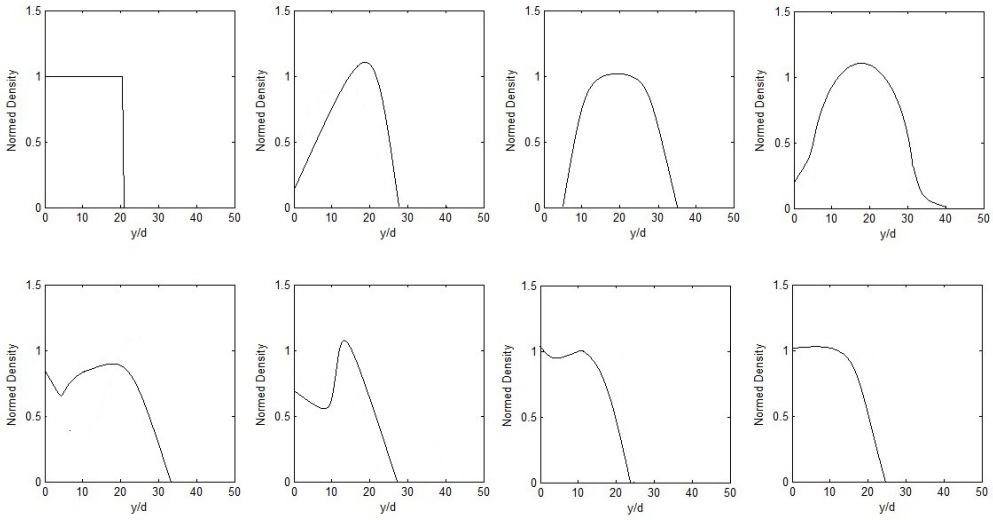

Figure 4.9 Denisty plots at various times due to a single tap of $a = 1.0d$ and $f = 10Hz$. $t = 0.4, 0.5, 0.55, 0.60, 0.70, 0.80, 0.90, 1.05$ respectively.

To demonstrate the effectiveness of the semidiscrete approach used, some comparisons between the trajectories from the numerical scheme and from discrete element simulations (DEM) are illustrated. The column comprises 20 spheres, each having a mass density $\rho = 1200kg/m^3$, loading stiffness $K = 1.366 \cdot 10^7 N/m$ and coefficient of restitution $e = 0.9$. Although it may be somewhat obscured by the difference in scales between the numerical solutions of (4.13) and the DEM simulations, the agreement of the numerical and simulation results is very good in each case.

The first comparison is for the case of a single tap of $a/d = 0.75$ and $f = 10Hz$. The half-sine tap begins at $t = 0.4s$. Figure 4.8 illustrates a set of density plots at various time. The trajectory integrated from the velocity field of numerical solution to the continuum BSR model could be find in figure 4.10; and DEM result is illustrated in figure 4.11. The two trajectories behave similarly. In addition, the top of the (continuum) column (corresponding to the top sphere in the simulations) and the top sphere both attain a maximum height of about $30d$ at approximately the same time.

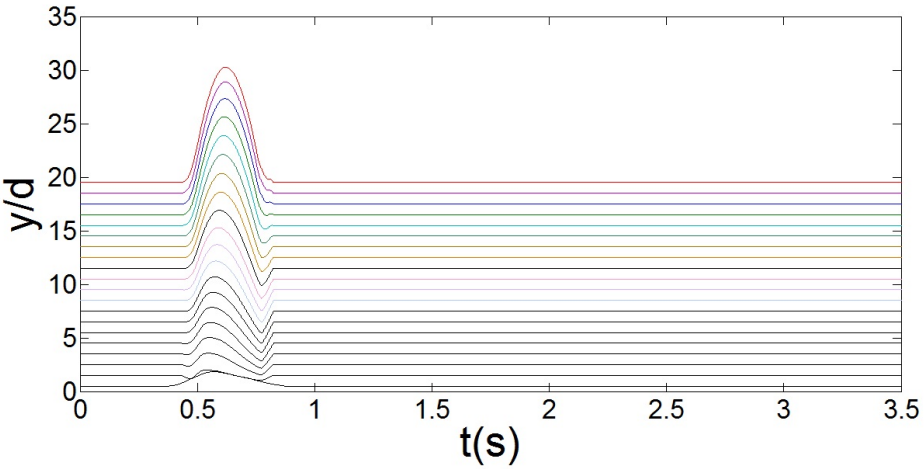

Figure 4.10 Trajectories due to single tap with $a = 0.75d$ and $f = 10Hz$ from semidiscrete simulation of BSR system.

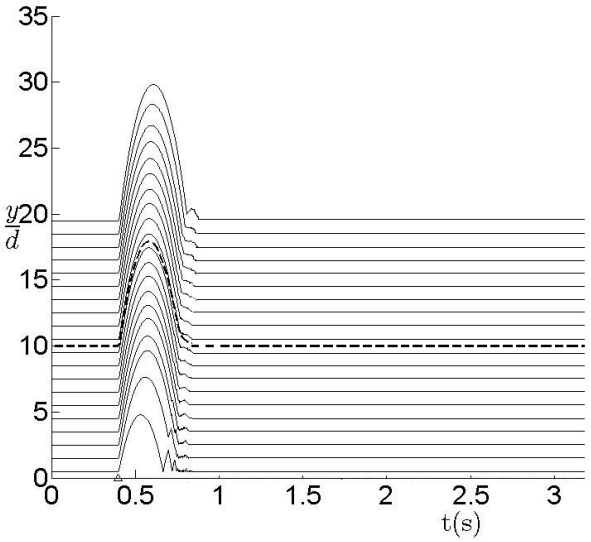

Figure 4.11 Trajectories due to single tap with $a = 0.75d$ and $f = 10Hz$ from DEM simulation. The dark line is the mass center trajectory.

In the second comparison, the amplitude of the single tap is increased to $a/d = 1.0$, with an unchanged frequency $f = 10Hz$. Figure 4.9 shows a set of density plots at various times. The trajectory integrated from the velocity field of numerical solution to the continuum BSR model can be found in Figure 4.12; and DEM result is illustrated in Figure 4.13. The top sphere center and the top of the continuum column reach a maximum height of about $38d$ in roughly the same period of time.

After the previous experiments, the focus of comparisons shall be for the case of multi-taps. For $a/d = 0.75$ and $f = 10hz$, the trajectory integrated from the velocity field of numerical solution to the continuum BSR model can be found in Figure 4.14; and DEM result is illustrated in Figure 4.15. The arrows (Figure 4.14) and the triangles (Figure 4.15) shows the time when a new tap is kicking in. Figure 4.16 and Figure 4.17 displays the results for $a = 1.0d$.

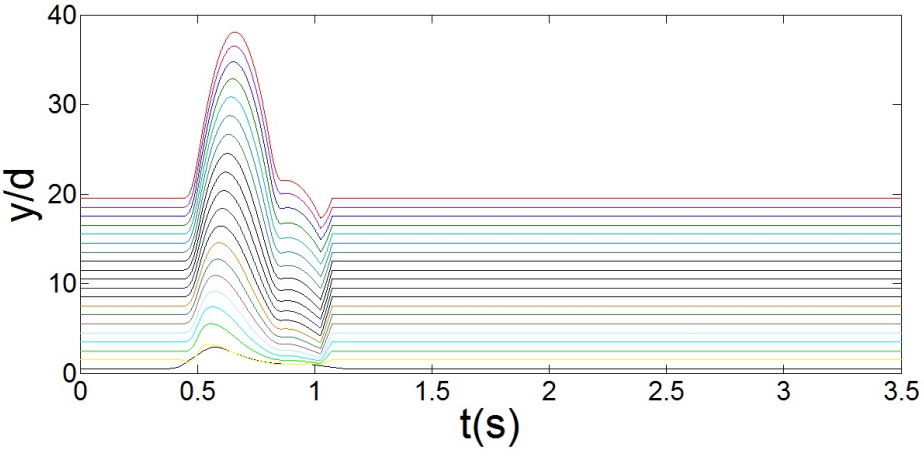

Figure 4.12 Trajectories due to single tap with $a = 1.0d$ and $f = 10Hz$ from semidiscrete simulation of BSR system.

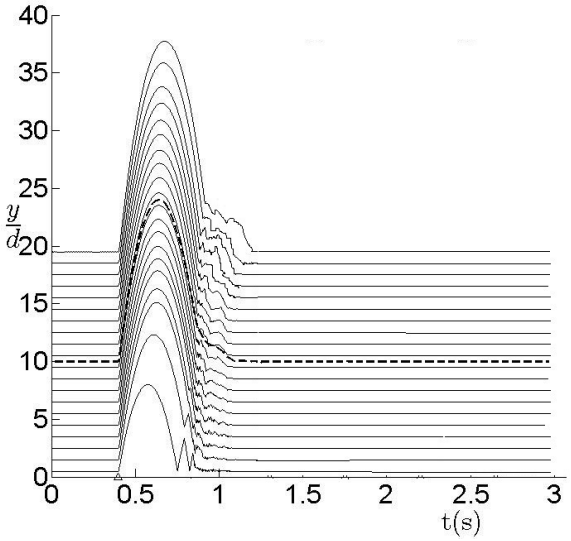

Figure 4.13 Trajectories due to single tap with $a = 1.0d$ and $f = 10Hz$ from DEM simulation.

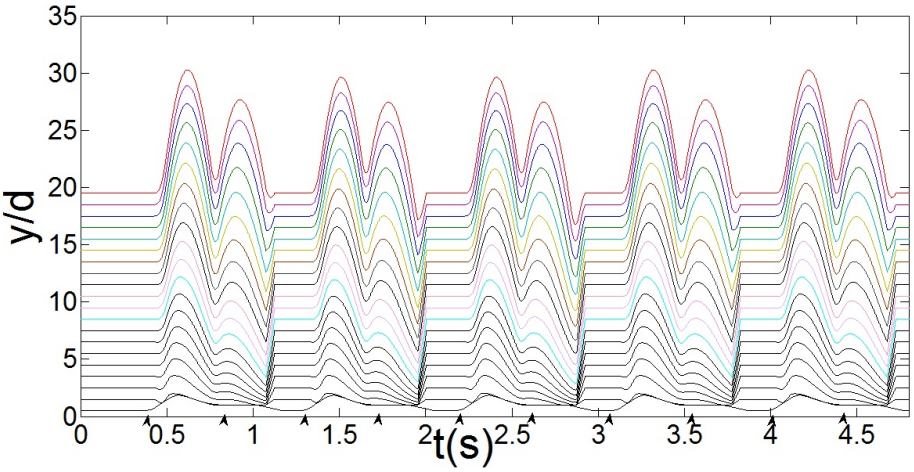

Figure 4.14 Trajectories due to multi-taps with $a = 0.75d$ and $f = 10Hz$ from semidiscrete simulation of BSR system. The arrows on the horizontal axis indicate the instant when a tap was applied to the column.

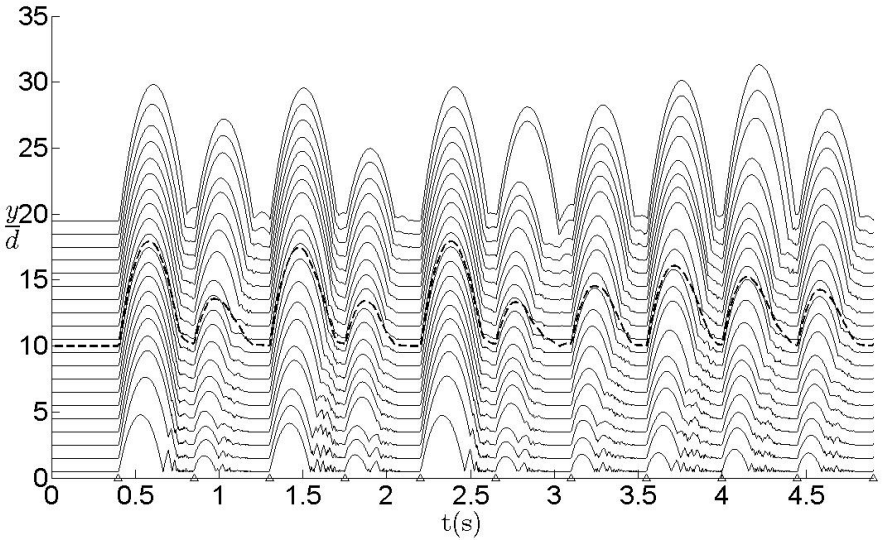

Figure 4.15 Simulated trajectories of the column as a function of time t at tap amplitude $a/d = 0.75$ and $f = 10Hz$. The diamonds on the horizontal axis indicate the instant when a tap was applied to the column. The dark line is the mass center trajectory.

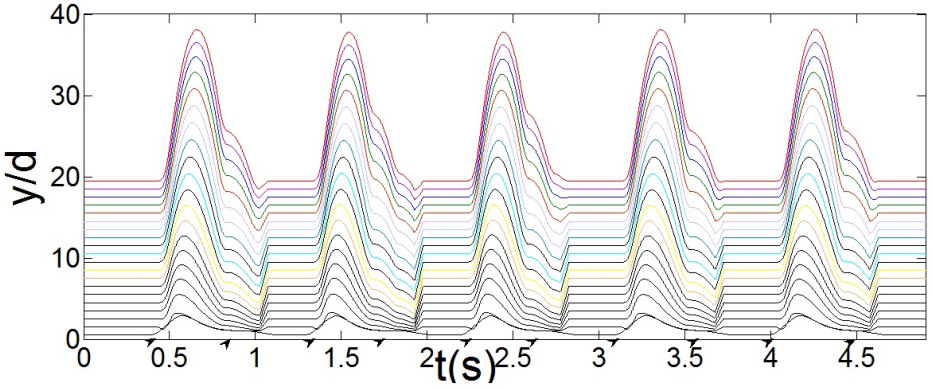

Figure 4.16 Trajectories due to multi-taps with $a = 1.0d$ and $f = 10Hz$ from semidiscrete simulation of BSR system. The arrows on the horizontal axis indicate the instant when a tap was applied to the column.

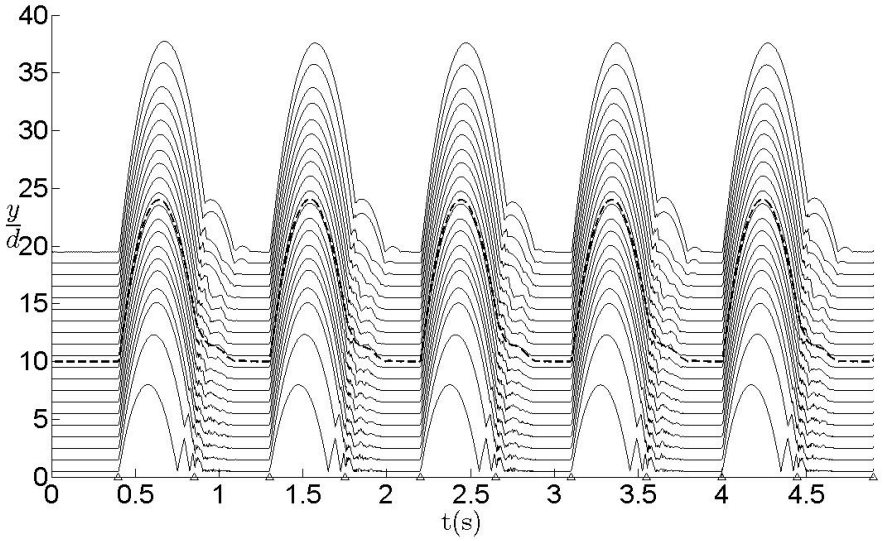

Figure 4.17 Simulated trajectories of the column as a function of time t at tap amplitude $a/d = 1.0$ and $f = 10Hz$. The diamonds on the horizontal axis indicate the instant when a tap was applied to the column. The dark line is the mass center trajectory.

CHAPTER 5

NUMERICAL ANALYSIS OF THE SEMIDISCRETE SCHEME

In this chapter, various important properties such as accuracy and stability shall analyzed insofar as they pertain to the scheme developed to numerically solve the BSR equations. An overview of basic definitions and fundamental results is given. Secondly, the accuracy of the semidiscrete numerical scheme is shown to be of order three in time and order two in space under the usual continuity assumptions. Thirdly, a brief introduction of Fourier analysis, and then the amplification factor method is described in order to study the von Neumann stability. In the last section, a detailed stability analysis is implemented to study the linearized BSR system.

5.1 Convergence, Consistency and Stability for Numerical Schemes

The most fundamental property that a numerical scheme must have in order to be useful to solve the corresponding partial differential equation is that its solutions should approximate the solution of the PDE and that this approximation improves as the grid spacing, h and k (usually are time and spatial mesh), tend to zero [47, 53]. Finite difference schemes, for example, will be discussed to illustrate the basic numerical concepts.

Definition 5.1 (Convergence [47]). *A one-step finite difference scheme approximating a partial differential equation is a convergent scheme if for any solution to the partial differential equation, $u(t,x)$, and solutions to the finite difference scheme, v_m^n, such that v_m^0 converges to $u_0(x)$ as mh converges to x, then v_m^n converges to $u(t,x)$ as (nk, mh) converges to (t,x) as h , k converge to* 0.

Proving that a given scheme is convergent is not easy, in general, if attempted in a direct manner. However, there are two related concepts that are relatively easy to check: consistency and stability.

Definition 5.2(Consistency [47]). *Given a partial differential equation $Pu = f$, and a finite difference scheme, $P_{k,h}v = f$, we say that the finite difference scheme is consistent with the partial differential equation if for any smooth function $\phi(t,x)$,*

$$P\phi - P_{k,h}\phi \to 0$$

as $k, h \to 0$, the convergence being pointwise convergence at each point (t,x).

Consistency implies that the solution of the partial differential equation, if it is smooth, is an approximate solution of the finite difference scheme. Similarly, convergence means that a solution of the finite difference scheme approximates a solution of the partial differential equation. It is natural to consider whether consistency is sufficient for a scheme to be convergent. Consistency is certainly necessary for convergence, but not sufficient.

The most important property that is required is stability. If a scheme is convergent, as v_m^n converges to $u(t,x)$, then certainly v_m^n is bounded in some sense. This is the essence of stability. The following definition of stability is for the homogeneous initial value problem.

Definition 5.3 (Stability [47]). *A finite difference scheme $P_{k,h}v_m^n$ for a first-order equation is stable in a stability region Λ if there is an integer J such that for any positive time T,there is a constant C_T such that*

$$h\sum_{m=-\infty}^{\infty}|v_m^n|^2 \le C_T h\sum_{j=0}^{J}\sum_{m=-\infty}^{\infty}|v_m^j|^2$$

for $0 \le nk \le T$, with $(k,h) \in \Lambda$.

The concept of stability for finite difference schemes is closely related to the concept of well-posedness for initial value problems for partial differential equations.

Definition 5.4 (Well-posedness [47]). *The initial value problem for the first-order partial differential equation $Pu = 0$ is well-posed if for any time $T \geq 0$, there is a constant C_T such that any solution $u(t, x)$ satisfies*

$$\int_{-\infty}^{\infty} |u(t,x)|^2 dx \leq C_T \int_{-\infty}^{\infty} |u(0,x)|^2 dx$$

for $0 \leq nk \leq T$.

The importance of the concepts of consistency and stability is seen in the Lax-Richtmyer equivalence theorem [27], which is a fundamental theorem in the theory of finite difference schemes for linear initial value problems. It shows that a consistent finite difference scheme for a linear partial differential equation for which the initial value problem is well-posed is convergent if and only if it is stable. Thus by using the Lax–Richtmyer Equivalence Theorem, the more difficult result – convergence – is replaced by the equivalent and generally more easily verifiable conditions of consistency and stability.

In addition, the following theorem should be mentioned, which can be generalized - at least in an approximate (linearized) sense - to more general systems using von Neumman analysis:

Theorem 5.1. [47] *A consistent one-step scheme for the equation* :

$$u_t + au_x + bu = 0 \tag{5.1}$$

is stable if and only if for this equation when b is equal to 0.

A similar result applies to many equations of the form (5.1) with variable coefficients [49].

The term stability here is the numerical stability, not the dynamical stability. Dynamical stability refers to the property of the system in which small variations from a reference state will decay, or at least not grow, with time. Numerical stability always means the behavior of solutions of the approximating numerical scheme are such that the magnitude of the local errors do not grow over a finite interval of time as the grid is refined, and the stability criteria are usually framed in terms of bounds on numerical mesh ratios. This can be clearly seen from the above theorem, the numerical stability is independent of the value b; however the equation 5.1 cannot be dynamically stable for negative b since any solutions grow without bound as t increase.

One general applicable procedure to deal with the variable coefficient is that one considers each of the *frozen coefficient* linear problems arising from the scheme. This is especially relevant for the BSR model, which is essentially a quasilinear hyperbolic system. The *frozen coefficient* problems are the constant coefficient problems obtained by fixing the coefficients of a linear system at their values attained at each point in the domain of the computation. For general nonlinear systems, complete numerical stability results are usually unattainable, so one typically linearizes the system about a simple solution and then employs the frozen coefficient approach. If each frozen coefficient problem is stable, then the variable coefficient problem is likely to be stable. Some detailed research related to the linear *frozen coefficient* problems could be found in the works of Kreiss [26], Shintani and Toemeda [45], Yamaguti and Nogi [56].

For example, the Lax-Friedrichs scheme applied to $u_t + a(t,x)u_x = 0$ is

$$v_m^{n+1} = \frac{1}{2}(v_{m+1}^n + v_{m-1}^n) - \frac{1}{2}a(t_n, x_m)\lambda(v_{m+1}^n + v_{m-1}^n),$$

where $\lambda = \frac{\Delta t}{\Delta x}$. The stability condition for this scheme is that the corresponding Courant–Friedrichs–Lewy (CFL) condition [14] $|a(t_n, x_m)| \cdot \lambda \leq 1$ be satisfied for all values of (t_n, x_m) in the domain of computation.

5.2 Convergence Analysis for Semidiscrete Scheme: Error Estimates

In this section, it shall be shown that the accuracy of the semidiscrete numerical method used to obtain approximate solutions system is of order three in time and order two in space under the usual assumptions of continuity of the derivatives of sufficiently high order of the system and its solutions. Although, the numerical scheme has been developed and fully implemented only for the case of one space dimension, the estimates shall be derived for n-dimensional space, since there is no real additional difficulty in doing so.

These properties shall be proved for the following system, which based on the above discussion subsumes the complete BSR model if the interaction kernel is velocity translation invariant and any applied motion depends only on the time t and possibly a parameter vector μ :

$$\begin{aligned} \boldsymbol{u}_t &= \boldsymbol{\alpha}\left(\boldsymbol{x}, t; \boldsymbol{\mu}\right) - \langle \boldsymbol{u}, \nabla \rangle \boldsymbol{u} + \int_{B_r(\boldsymbol{x})} \rho(\boldsymbol{y}, t) \boldsymbol{\Theta}\left(\boldsymbol{x}, \boldsymbol{y}, \boldsymbol{u}(\boldsymbol{x}, t), \boldsymbol{u}(\boldsymbol{y}, t)\right) d\boldsymbol{y}, \\ \rho_t &= -\left[\langle u, \nabla \rangle \rho + \rho \operatorname{div} \boldsymbol{u}\right], \end{aligned} \tag{5.2}$$

which is subject to the initial conditions

$$\boldsymbol{u}(\boldsymbol{x}, 0) = \boldsymbol{u}_0(\boldsymbol{x}), \rho(\boldsymbol{x}, 0) = \rho_0(\boldsymbol{x}), \ \boldsymbol{x} \in \Omega, \tag{5.3}$$

where Ω is a fixed, smooth submanifold of $\mathbb{R}^n$ with boundary $\partial\Omega$ and the system is defined for $\Omega \times [0, \infty)$. Here the function $\boldsymbol{\alpha}$ represents the external and any inertial forces present. In keeping with the semidiscrete method employed, it is convenient to recast the above initial value problem in the form of the following functional ODE:

$$\frac{d\boldsymbol{v}}{dt} = \boldsymbol{G}\left(\boldsymbol{x}, t, \boldsymbol{v}, \boldsymbol{v}_{\boldsymbol{x}}; \mu\right), \tag{5.4}$$

subject to the initial functional value

$$\boldsymbol{v}(0) = \boldsymbol{v}_0, \tag{5.5}$$

where $\boldsymbol{v} := (\boldsymbol{u}, \rho)$, $\boldsymbol{v}_0 := (\boldsymbol{u}_0, \rho_0)$ and

$$\boldsymbol{G}(\boldsymbol{x}, t, \boldsymbol{v}, \boldsymbol{v}_{\boldsymbol{x}}; \mu) := \Bigg(\boldsymbol{\alpha}(\boldsymbol{x}, t; \boldsymbol{\mu}) - \langle \boldsymbol{u}, \nabla \rangle \boldsymbol{u} + \int_{B_r(\boldsymbol{x})} \rho(\boldsymbol{y}, t) \boldsymbol{\Theta}(\boldsymbol{x}, \boldsymbol{y}, \boldsymbol{u}(\boldsymbol{x}, t), \boldsymbol{u}(\boldsymbol{y}, t))\, d\boldsymbol{y}, \\ - \left[\langle u, \nabla \rangle \rho + \rho \operatorname{div} \boldsymbol{u} \right] \Bigg) \tag{5.6}$$

Note that here $\boldsymbol{v}(t)$ is a map from Ω to $\mathbb{R}^{n+1}$ for every $t \in [0, \infty)$, so it shall also be denoted as $\boldsymbol{v}(t, \boldsymbol{x})$ when convenient to do so.

In what follows, it assumed that the functions in (5.4)-(5.5) and the solution have uniformly bounded derivatives of all orders less than or equal to five. The discrete times for the third order Runge–Kutta (RK3) solution are denoted as $0 = t_0 < t_1 < t_2 < \cdots$, or $\{t_i\}$ and the mesh points for the (central difference) space discretization are defined as $\{x_j\}$, where $j = (j_1, \ldots, j_n)$ is naturally a multi-index. The time and space increments are taken to be uniform and are defined as h and l, respectively. For the purpose of describing the moving average employed in the scheme, it is convenient to introduce the near-neighbor average of a (scalar or vector) quantity (or function) q_j as

$$NA(q_j) := \frac{1}{4n} \left[2nq_j + \sum\nolimits_{k=1}^{n} q_{j \pm e_k} \right], \tag{5.7}$$

where the e_k represent the standard basis in $\mathbb{R}^{n+1}$; namely, $e_1 := (1, 0, 0, \ldots, 0, 0)$, $e_2 := (0, 1, 0, \ldots, 0, 0)$, $\ldots$, $e_n := (0, 0, 0, \ldots, 0, 1)$. Let the central difference approximation to $\boldsymbol{G}$ centered at $x = x_j$, where for example $\partial_{x_k} u_1(t, \boldsymbol{x}_j)$ is approximated by

$$\frac{u_1(t, \boldsymbol{x}_{j+e_k}) - u_1(t, \boldsymbol{x}_{j-e_k})}{2l} = \partial_{x_k} u_1(t, \boldsymbol{x}_j) + O\left(l^2\right),$$

be denoted as $\boldsymbol{G}_j$. Then it follows from the assumptions on the derivatives that

$$\boldsymbol{G}_j = \boldsymbol{G} + O\left(l^2\right) \tag{5.8}$$

uniformly on $\Omega \times [0, T)$ for any finite positive time T.

The semidiscrete, three-point moving average scheme, which is identical to the near neighbor moving average when $n = 1$, together with RK3 integration is based on solving the following system of ODEs for all multi-indices comprising the space discretization:

$$\frac{d\hat{\boldsymbol{V}}_j}{dt} = \hat{\boldsymbol{G}}_j, \tag{5.9}$$

subject to the initial condition

$$\hat{\boldsymbol{V}}_j(0) = \boldsymbol{v}(0, \boldsymbol{x}_j), \tag{5.10}$$

where

$$\hat{\boldsymbol{G}}_j := NA\left(\boldsymbol{G}\left(x_j, t, \hat{\boldsymbol{V}}_j, \delta\hat{\boldsymbol{V}}_j; \mu\right)\right) \tag{5.11}$$

and $\delta\boldsymbol{V}_j$ is the analog of a central difference approximation of $\partial_{\boldsymbol{x}}\boldsymbol{V}_j$, which is a matrix comprising all vector entries of the form

$$\frac{\hat{\boldsymbol{V}}_{j+e_k} - \hat{\boldsymbol{V}}_{j-e_k}}{2l},\ 1 \le k \le n.$$

If the approximations produced by using RK3 on (5.9) are denoted by $\boldsymbol{V}_j^i$, it follows from standard Runge–Kutta estimates (*cf.* [2, 39]) and the assumptions on smoothness of $\boldsymbol{G}$ that the local truncation error is

$$\hat{\boldsymbol{V}}_j(t_i) - \hat{\boldsymbol{V}}_j^i = O(h^4), \tag{5.12}$$

and the global truncation error is

$$\hat{\boldsymbol{V}}_j(t_i) - \hat{\boldsymbol{V}}_j^i = O(h^3). \tag{5.13}$$

The following result is useful for the completion of the error analysis.

Lemma 5.1 *Let $f : U_j \to \mathbb{R}$ be a C^2 function, where U_j is an open set in $\mathbb{R}^n$ containing $\boldsymbol{x}_j$ and all its near-neighbor points. Then*

$$NA\left(f(\boldsymbol{x}_j)\right) = f(\boldsymbol{x}_j) + O(l^2).$$

Proof. According to (5.7), the near-neighbor average can be rewritten as

$$NA\left(f(\boldsymbol{x}_j)\right) = \frac{1}{4n}\left[2nf(\boldsymbol{x}_j) + \sum\nolimits_{k=1}^{n}\left(f(\boldsymbol{x}_{j+e_k}) + f(\boldsymbol{x}_{j-e_k})\right)\right].$$

Then, using a Taylor expansion and the smoothness hypothesis, one obtains for each $1 \le k \le n$ the representation

$$\begin{aligned} f(\boldsymbol{x}_{j+e_k}) + f(\boldsymbol{x}_{j-e_k}) &= \left(f(\boldsymbol{x}_j) + \partial_k f(\boldsymbol{x}_j) l + O(l^2)\right) + \left(f(\boldsymbol{x}_j) + \partial_k f(\boldsymbol{x}_j)(-l) + O(l^2)\right) \\ &= 2f(\boldsymbol{x}_j) + O(l^2), \end{aligned}$$

which when substituted in the above formula yields

$$NA\left(f(\boldsymbol{x}_j)\right) = \frac{1}{4n}\left[2nf(\boldsymbol{x}_j) + n\left(2f(\boldsymbol{x}_j) + O(l^2)\right)\right] = f(\boldsymbol{x}_j) + O(l^2),$$

thereby completing the proof. □

To complete the error analysis, one denotes the RK3 approximations for the system

$$\frac{d\boldsymbol{v}_j}{dt} := \frac{d\boldsymbol{v}(t, \boldsymbol{x}_j)}{dt} = \boldsymbol{G}\left(\boldsymbol{x}_j, t, \boldsymbol{v}, \boldsymbol{v}_{\boldsymbol{x}}; \mu\right)$$

as $\boldsymbol{v}_j^i$ and the RK3 approximations for the system

$$\frac{d\boldsymbol{V}_j}{dt} = \boldsymbol{G}\left(\boldsymbol{x}_j, t, \boldsymbol{V}_j, \delta\boldsymbol{V}_j; \mu\right)$$

as $\boldsymbol{V}_j^i$. Then one computes that the local truncation error for the complete semidiscrete moving average RK3 scheme is

$$E_j^i := \left|\boldsymbol{v}(t_i, \boldsymbol{x}_j) - \hat{\boldsymbol{V}}_j^{\,i}\right| \le \left|\boldsymbol{v}(t_i, \boldsymbol{x}_j) - \boldsymbol{v}_j^i\right| + \left|\boldsymbol{v}_j^i - \boldsymbol{V}_j^i\right| + \left|\boldsymbol{V}_j^i - \hat{\boldsymbol{V}}_j^{\,i}\right|.$$

Whence, it follows from the overall smoothness assumptions, the above definitions, the standard Runge–Kutta truncation errors, Lemma 5.1, (5.8) and (5.12) that

$$E_j^i \leq O(h^4) + O\left(l^2\right) + O\left(l^2\right) = O(h^4) + O\left(l^2\right).$$

And finally from the standard local to global estimates for Runge–Kutta errors [2, 39], one finds that the global truncation error for the semidiscrete moving average RK3 scheme is

$$E_j = O(h^3) + O\left(l^2\right),$$

which confirms that the error is of order h^3 in time and l^2 in space.

5.3 Introduction to von Neumann Analysis

Von Neumann's stability analysis is a widely used (back-of-the-envelope) analytical procedure for determining the (numerical) stability properties of a numerical method applied to a PDE that does not account for the boundary conditions. The technique works for linear, constant coefficient differential equations that are discretized on uniformly spaced grids. It also provides useful - although not rigorous - stability criteria for nonlinear systems via linearizing and freezing coefficients. This is the method that shall be employed here to analyze the stability of the semi-discrete scheme for the BSR model in one space dimension. The tool that is used most extensively in von Neumann stability analysis is Fourier analysis [46] [47]. Fourier analysis is used on both the real line R and on the grid of integers Z or hZ, which is defined by $hZ = \{hm : m \in Z\}$. For a function $u(x)$ defined on the real line R, its Fourier transform $\bar{u}(w)$ is defined by

$$\bar{u}(w) = \frac{1}{\sqrt{2\pi}} \int_{-\infty}^{\infty} e^{-iwx} u(x) dx. \tag{5.14}$$

The Fourier transform of u is a function of the real variable w and is uniquely defined by u. The function $\bar{u}$ is an alternative representation of the function u. Information about certain properties of u can be inferred from the properties of $\bar{u}$. For example, the rate at which $\bar{u}$ decays for large values of w is related to the number of derivatives that u has.

The Fourier inversion formula, given by

$$u(x) = \frac{1}{\sqrt{2\pi}} \int_{-\infty}^{\infty} e^{iwx} \bar{u}(w) dw, \tag{5.15}$$

shows how u can be recovered from $\bar{u}$. The Fourier inversion formula expresses the function u as a superposition of waves, given by e^{-iwx}, with different amplitudes $\bar{u}(w)$. Notice that $\bar{u}(w)$ may be complex valued even if $u(x)$ is real valued.

In a similar fashion, if v is a grid function defined for all integers m, its Fourier transform is given by

$$\bar{v}(\xi) = \frac{1}{\sqrt{2\pi}} \sum_{m=-\infty}^{\infty} e^{-im\xi} v_m \tag{5.16}$$

for $\xi \in [-\pi, \pi]$, and $\bar{v}(-\pi) = \bar{v}(\pi)$. The Fourier inversion formula is given by

$$v_m = \frac{1}{\sqrt{2\pi}} \int_{-\pi}^{\pi} e^{im\xi} \bar{v}(\xi) d\xi, \tag{5.17}$$

Fourier analysis on the integers Z is the same as the study of Fourier series representations of functions defined on an interval. From the perspective of Fourier series one usually starts with a function $\bar{v}(\xi)$ defined on the interval $[\pi, \pi]$ and shows that it can be represented as a series such as (5.16) with coefficients v_m given by (5.17). In general study of finite difference schemes it is more natural to start with the grid functions v_m and regard the formula (5.17) as a representation of the grid function. The two approaches are mathematically equivalent. The Fourier inversion formula (5.17) has an interpretation, analogous to (5.15), as expressing v as a superposition of waves.

If the spacing between the grid points is h, one can change variables and define the transform by

$$\bar{v}(\xi) = \frac{1}{\sqrt{2\pi}} \sum_{m=-\infty}^{\infty} e^{-imh\xi} v_m h \tag{5.18}$$

for $\xi \in [\pi/h, \pi/h]$ and then the inversion formula is

$$v_m = \frac{1}{\sqrt{2\pi}} \int_{-\pi/h}^{\pi/h} e^{imh\xi} \bar{v}(\xi) d\xi, \tag{5.19}$$

Using Fourier analysis one can give necessary and sufficient conditions for the stability of finite difference schemes. It also can and shall be used in the sequel to analyze semidiscrete schemes by treating the time evolution as iterations of the difference formulas used for the space variables. The method will be illustrated by considering a following example. Through the use of the Fourier transform, the determination of the stability of a scheme is reduced to relatively simple algebraic considerations. The forward-time backward-space scheme for 1-D wave equation $u_t + au_x = 0$ is,

$$\frac{v_m^{n+1} - v_m^n}{k} + a\frac{v_m^n - v_{m-1}^n}{h} = 0,$$

which can be rewritten as

$$v_m^{n+1} = (1 - a\lambda)v_m^n + a\lambda v_{m-1}^n, \tag{5.20}$$

where $\lambda = k/h, k = \Delta t$ and $h = \Delta x$. Using the Fourier inversion formula (5.19) for v_n, one obtains

$$v_m^n = \frac{1}{\sqrt{2\pi}} \int_{-\pi/h}^{\pi/h} e^{imh\xi} \bar{v}^n(\xi) d\xi,$$

and substituting this in (5.20) for v_m^n and v_{m-1}^n yields

$$v_m^{n+1} = \frac{1}{\sqrt{2\pi}} \int_{-\pi/h}^{\pi/h} e^{imh\xi} [(1 - a\lambda) + a\lambda e^{-ih\xi}] \bar{v}^n(\xi) d\xi \tag{5.21}$$

Comparing this formula with the Fourier inversion formula for v_{n+1},

$$v_m^{n+1} = \frac{1}{\sqrt{2\pi}} \int_{-\pi/h}^{\pi/h} e^{imh\xi} \bar{v}^{n+1}(\xi) d\xi,$$

and using the fact that the Fourier transform is unique, it follows that the integrand of (5.21) is the same as that in the inversion formula. Consequently,

$$\bar{v}^{n+1}(\xi) = [(1 - a\lambda) + a\lambda e^{-ih\xi}]\bar{v}^n(\xi) = g(h\xi)\bar{v}^n(\xi) \tag{5.22}$$

where $g(h\xi) = (1 - a\lambda) + a\lambda e^{-ih\xi}$

The formula (5.22) shows that advancing the solution of the scheme by one time step is equivalent to multiplying the Fourier transform of the solution by the amplification factor $g(h\xi)$. The *amplification factor* is so called because its magnitude is the amount that the amplitude of each frequency in the solution, given by $\bar{v}^n(\xi)$, is increased in advancing the solution one time step. From (5.22) one obtains the important formula

$$\bar{v}^n(\xi) = [g(h\xi)]^n \bar{v}^0(\xi) \tag{5.23}$$

Note that the superscript on v is an index of the time level, while on g it is a power. By means of the Fourier transform every one-step scheme can be put in the form (5.23), and this provides a standard method for studying the wide variety of schemes[47]. All the information about a scheme is contained in its amplification factor, and it is shown above how to extract important information from it. In particular, the stability and accuracy of schemes is easy to determine from the amplification factor.

It follows from the above theoretical developments that to determine the stability of a finite difference scheme it suffices to consider the amplification factor $g(h\xi)$. This observation is due to von Neumann, and because of that, this analysis is usually called von Neumann analysis.

One need not write out the integrals and obtain expressions such as (5.21) to find the amplification factor g. A simpler and equivalent procedure is to replace v_m^n in the scheme by $[g(\theta)]^n e^{im\theta}$ for each value of n and m , where $\theta = h\xi$. The resulting equation can then be solved for the amplification factor.

In the following example, a forward-time central-space scheme to deal with the 1-D wave equation $u_t + au_x = 0$ will be shown to be unstable using the method illustrated above.

$$\frac{v_m^{n+1} - v_m^n}{k} + a\frac{v_{m+1}^n - v_{m-1}^n}{2h} = 0,$$

Replacing v_m^n by $g^n e^{im\theta}$, the preceding expression is transformed to

$$\frac{g^{n+1}e^{im\theta} - g^n e^{im\theta}}{k} + a\frac{g^n e^{i(m+1)\theta} - g^n e^{i(m-1)\theta}}{2h} = 0$$

i.e.

$$\begin{aligned}
g^{n+1}e^{im\theta} &= g^n e^{im\theta} - \frac{1}{2}a\frac{k}{h}[g^n e^{i(m+1)\theta} - g^n e^{i(m-1)\theta}] \\
&= g^n e^{im\theta} - \frac{1}{2}a\frac{k}{h}g^n e^{im\theta}[e^{i\theta} - e^{-i\theta}] \\
&= g^n e^{im\theta}[1 - \frac{1}{2}a\frac{k}{h}(e^{i\theta} - e^{-i\theta})] \\
&= g^n e^{im\theta}[1 - \frac{1}{2}a\frac{k}{h}(\cos\theta + i\sin\theta - \cos\theta + i\sin\theta] \\
&= g^n e^{im\theta}[1 - ia\frac{k}{h}\sin\theta]
\end{aligned}$$

which gives

$$g = 1 - ia\lambda\sin\theta.$$

where $\lambda := \frac{\Delta t}{\Delta x} = \frac{k}{h}$.

The determination of the amplification factor by replacing v_m^n in the scheme by $[g(\theta)]^n e^{im\theta}$ is not just for looking for solutions of the difference scheme that have the form $v_m^n = [g(\theta)]^n e^{im\theta}$. The replacement is a shortcut in the method used at

the beginning of the section, in which it was shown that all solutions of the one-step difference scheme were given by formula (5.23), and this demonstration actually gave the form of the amplification factor. That same procedure can be applied to any one-step scheme to determine the form of the amplification factor. A rearrangement of the manipulations used to determine the amplification factor shows that the two procedures are equivalent in determining the form of the amplification factor

5.4 Stability Analysis of the Linearized BSR Equations

The linearized frozen coefficient equation $u_t + au_x = f(x,t)$ can be rewritten as $u_t = -au_x + f$. In this dissertation, u_m^n is written for the value of u at the grid point $(t_n, x_m) := (n\Delta t, m\Delta x)$. When the first order Runge–Kutta coupled with two-mesh central difference is implemented, the difference scheme is

$$\frac{u_m^{n+1} - u_m^n}{\Delta t} = -a\frac{u_{m+1}^n - u_{m-1}^n}{2\Delta x} + f_m^n$$

or

$$u_m^{n+1} = u_m^n - \frac{1}{2}a\frac{\Delta t}{\Delta x}(u_{m+1}^n - u_{m-1}^n) + \Delta t f_m^n$$

which is equivalent to the forward time central space scheme. By applying the amplification factor and by ignoring the f_m^n term in the von Neumann stability analysis, it is easy to get

$$g = 1 - ia\lambda \sin\theta,$$

where $\lambda = \frac{\Delta t}{\Delta x}$. As a result, the amplitude square of the amplification factor

$$|g|^2 = 1 + a^2\lambda^2 \sin^2\theta \geq 1$$

for any possible value of θ, which means that the first order R-K with central difference is unstable.

However, in the following, it will be shown that the first order R-K with central difference is stable under its corresponding CFL condition, if a moving average is applied. Written as two separate steps, the scheme is

$$\bar{u}_m^{n+1} = u_m^n - \frac{1}{2}a\lambda(u_{m+1}^n - u_{m-1}^n) + \Delta t f_m^n$$
$$u_m^{n+1} = \frac{1}{4}(\bar{u}_{m+1}^{n+1} + 2\bar{u}_m^{n+1} + \bar{u}_{m-1}^{n+1}).$$

To apply von Neumann analysis to this scheme, one can eliminate all reference to the intermediate quantity $\bar{u}$, obtaining an equation for u_m^{n+1} in terms of $u_{m'}^n$ for m' ranging from $m-2$ to $m+2$. Here an equivalent and simpler procedure is used, which is to replace all occurrences of $\bar{u}_m^{n+1}$ by $\bar{g}g^n e^{im\theta}$ as well as the usual replacement of u_m^n by $g^n e^{im\theta}$. Again by ignoring the f_m^n term as in the previous calculation, one obtains

$$\bar{g} = 1 - ia\lambda \sin\theta.$$

and

$$\begin{aligned} g &= \frac{1}{4}(e^{i\theta} + 2 + e^{-i\theta})\bar{g} \\ &= \frac{1}{4}(\cos\theta + i\sin\theta + 2 + \cos\theta - i\sin\theta)\bar{g} \\ &= \frac{1}{4}(2\cos\theta + 2)\bar{g} \\ &= \bar{g}\cos^2\frac{1}{2}\theta. \end{aligned}$$

Combining the previous two estimates, one finds that

$$|g|^2 = |\bar{g}|^2 \cos^4\frac{1}{2}\theta = (1 + a^2\lambda^2\sin^2\theta)\cos^4\frac{1}{2}\theta.$$

If one takes λ to be constant, then the stability requirement is that g have magnitude at most 1. Hence, for stability it must satisfy

$$(1 + a^2\lambda^2 \sin^2\theta) \cos^4 \frac{1}{2}\theta \leq 1.$$

i.e.

$$(1 + 4a^2\lambda^2 \sin^2 \frac{1}{2}\theta \cos^2 \frac{1}{2}\theta) \cos^4 \frac{1}{2}\theta \leq 1.$$

which is equivalent to

$$\begin{aligned} 4a^2\lambda^2 \sin^2 \frac{1}{2}\theta \cos^2 \frac{1}{2}\theta \cos^4 \frac{1}{2}\theta &\leq 1 - \cos^4 \frac{1}{2}\theta \\ &= (1 - \cos^2 \frac{1}{2}\theta)(1 + \cos^2 \frac{1}{2}\theta) \\ &= \sin^2 \frac{1}{2}\theta(1 + \cos^2 \frac{1}{2}\theta) \end{aligned}$$

By canceling the nonnegative $\sin^2 \frac{1}{2}\theta$, one gets

$$4a^2\lambda^2 \cos^6 \frac{1}{2}\theta \leq 1 + \cos^2 \frac{1}{2}\theta,$$

which must hold for all θ. When $\theta = 0$, a necessary condition $a^2\lambda^2 \leq \frac{1}{2}$ can be obtained. Actually this is also a sufficient. Since $\cos^2 \frac{1}{2}\theta \leq 1$,

$$4a^2\lambda^2 \cos^6 \frac{1}{2}\theta \leq 4 \cdot \frac{1}{2} \cdot \cos^6 \frac{1}{2}\theta \leq 2 \cos^2 \frac{1}{2}\theta \leq 1 + \cos^2 \frac{1}{2}\theta$$

It is shown that though the first order R-K with central difference(or forward-time central-space scheme) is unstable for solving the linearized partial differential equation, the scheme with the (moving average) smoother is stable and the corresponding Courant–Friedrichs–Levy (CFL) condition is

$$|a\lambda| \leq \frac{1}{\sqrt{2}}.$$

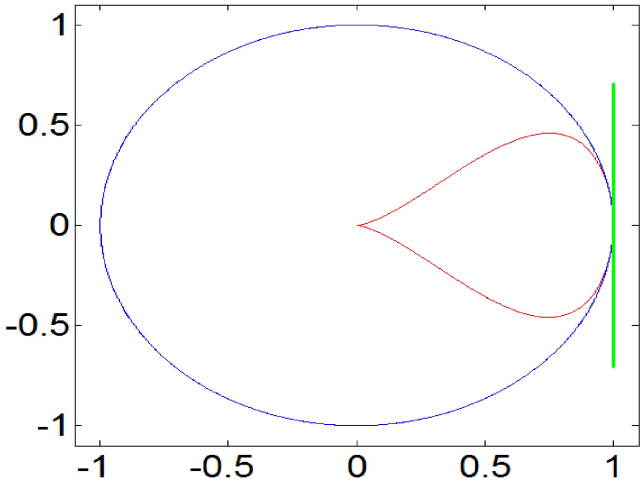

Figure 5.1 The images of $g(\theta)$. The blue curve is the unit circle. The green curve represents the $g(\theta)$ for semi-discrete scheme without the smoothing operator, while the red curve represents the $g(\theta)$ for the semi-discrete scheme with smoothing.

One can also infer from the previous argument that the averaging smoother is trying to relax the stability condition. Different averaging smoothers could be studied in the same manner.

Figure 5.1 shows the set of points of $g(\theta)$s. The blue curve is the unit circle. The green curve represent the $g(\theta)$ for semi-discrete scheme without the smoothing operator, while the red curve represent the $g(\theta)$ for semidiscrete scheme with smoothing. The red curve touches at 1 because $g(0) = 1$.

If a two stage R-K or Heun's method is implemented to deal with the time derivative, one can show that

$$K_1 = \Delta t(-au_x) = -a\Delta t u_x$$

$$K_2 = \Delta t[-a\bar{u}_x] = -a\Delta t[u + K_1]_x$$

$$= -a\Delta t u_x + a^2(\Delta t)^2 u_{xx}$$

The scheme before the smoother is applied applied is

$$u_m^{n+1} = u_m^n + \frac{1}{2}[K_1 + K_2]$$

or

$$u_m^{n+1} = u_m^n - a\Delta t \frac{u_{m+1}^n - u_{m-1}^n}{2\Delta x} + \frac{1}{2}a^2(\Delta t)^2 \frac{u_{m+1}^n + u_{m-1}^n - 2u_m^n}{(\Delta x)^2}$$

Notice that f is set to 0 as required to obtain the amplification factor.

Thus, the full scheme is

$$\bar{u}_m^{n+1} = u_m^n - a\Delta t \frac{u_{m+1}^n - u_{m-1}^n}{2\Delta x} + \frac{1}{2}a^2(\Delta t)^2 \frac{u_{m+1}^n + u_{m-1}^n - 2u_m^n}{(\Delta x)^2}$$
$$u_m^{n+1} = \frac{1}{4}(\bar{u}_{m+1}^{n+1} + 2\bar{u}_m^{n+1} + \bar{u}_{m-1}^{n+1}).$$

Similarly, one can get

$$\begin{aligned}\bar{g} &= 1 - \frac{a\lambda}{2}[e^{i\theta} - e^{-i\theta}] + \frac{1}{2}a^2\lambda^2[e^{i\theta} + e^{-i\theta} - 2] \\ &= 1 - ia\lambda \sin\theta + a^2\lambda^2(\cos\theta - 1) \\ &= [1 - 2a^2\lambda^2 \sin^2\frac{\theta}{2}] - ia\lambda \sin\theta\end{aligned}$$

and

$$g = \bar{g}\cos^2\frac{1}{2}\theta.$$

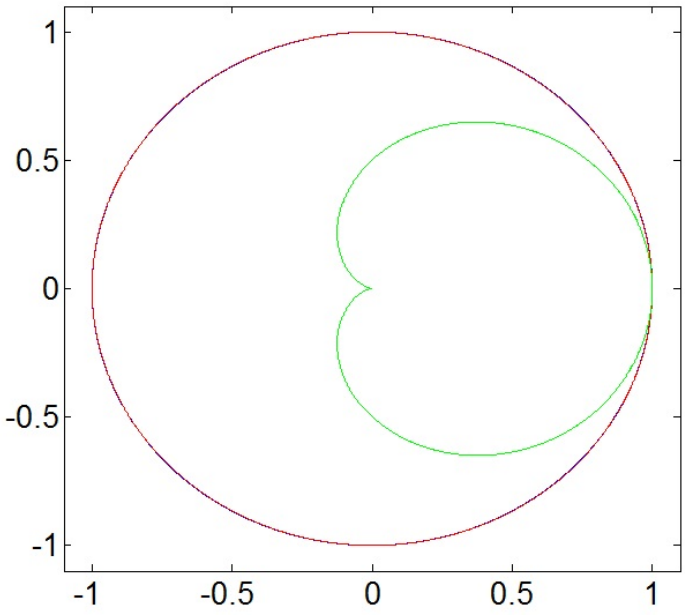

Figure 5.2 The images of $g(\theta)$. The blue curve is the unit circle. The red curve represents the $g(\theta)$ for semi-discrete scheme without the smoothing operator, which overlaps the unit circle. The green curve represents the $g(\theta)$ for semi-discrete scheme with smoothing.

$$
\begin{aligned}
|g(\theta)|^2 &= [(1-2a^2\lambda^2\sin^2\frac{1}{2}\theta)^2 + (a\lambda\sin\theta)^2]\cos^4\frac{1}{2}\theta. \\
&= [(1-2a^2\lambda^2\sin^2\frac{1}{2}\theta)^2 + (2a\lambda\sin\frac{1}{2}\cos\frac{1}{2}\theta)^2]\cos^4\frac{1}{2}\theta \\
&= [1-4a^2\lambda^2\sin^2\frac{1}{2}\theta + 4a^4\lambda^4\sin^4\frac{1}{2}\theta + 4a^2\lambda^2\sin^2\frac{1}{2}\theta\cos^2\frac{1}{2}\theta]\cos^4\frac{1}{2}\theta \\
&= [1-4a^2\lambda^2\sin^2\frac{1}{2}\theta(1-\cos^2\frac{1}{2}\theta) + 4a^4\lambda^4\sin^4\frac{1}{2}\theta]\cos^4\frac{1}{2}\theta \\
&= [1-4a^2\lambda^2\sin^4\frac{1}{2}\theta + 4a^4\lambda^4\sin^4\frac{1}{2}\theta]\cos^4\frac{1}{2}\theta \\
&= [1-4a^2\lambda^2(1-a^2\lambda^2)\sin^4\frac{1}{2}\theta]\cos^4\frac{1}{2}\theta
\end{aligned}
$$

From this form for $|g(\theta)|^2$, it is easy to verify that $|a\lambda| \leq 1$ is a necessary and sufficient stability condition.

Figure 5.2 shows the set of points of $g(\theta)$s for $|a\lambda| = 1$. The blue curve is the unit circle. The red curve represents the $g(\theta)$ for the semi-discrete scheme without smoothing, which overlaps the unit circle. The green curve represents the $g(\theta)$ for semi-discrete scheme with the smoothing operator. The green curve touches at 1 because $g(0) = 1$. In comparison to the red curve, the green curve covers a smaller region, with less possibility to touch 1. This confirms that the moving average smoothing filter improved the stability greatly.

Now a third order Runge-Kutta is implemented,

$$K_1 = \Delta t(-au_x) = -a\Delta t u_x$$

$$\begin{aligned} K_2 &= \Delta t[-a\bar{u}_x] = -a\Delta t[u + \frac{K_1}{2}]_x \\ &= -a\Delta t[u - \frac{1}{2}a\Delta t u_x]_x = -a\Delta t u_x + \frac{1}{2}a^2(\Delta t)^2 u_{xx} \end{aligned}$$

$$\begin{aligned} K_3 &= \Delta t[-a\bar{\bar{u}}_x] = -a\Delta t[u + 2K_2 - K_1]_x \\ &= -a\Delta t[u - 2a\Delta t u_x + a^2(\Delta t)^2 u_{xx} + a\Delta t u_x]_x \\ &= -a\Delta t[u - a\Delta t u_x + a^2(\Delta t)^2 u_{xx}]_x \\ &= -a\Delta t u_x + a^2(\Delta t)^2 u_{xx} - a^3(\Delta t)^3 u_{xxx} \end{aligned}$$

$$\begin{aligned} u^{n+1} &= u^n + \frac{1}{6}[K_1 + 4K_2 + K_3] \\ &= u^n - a\Delta t(u^n)_x + \frac{1}{2}a^2(\Delta t)^2(u^n)_{xx} - \frac{1}{6}a^3(\Delta t)^3(u^n)_{xxx} \end{aligned}$$

Hence, the full scheme of a third order R-K coupled with central space scheme and moving average smoother is

$$\begin{aligned}
\bar{u}_m^{n+1} &= u_m^n - a\Delta t \frac{u_{m+1}^n - u_{m-1}^n}{2\Delta x} \\
&\quad + \frac{1}{2}a^2(\Delta t)^2 \frac{u_{m+1}^n + u_{m-1}^n - 2u_m^n}{(\Delta x)^2} \\
&\quad - \frac{1}{6}a^3(\Delta t)^3 \frac{u_{m+2}^n - 2u_{m+1}^n + 2u_{m-1}^n - u_{m-2}^n}{2(\Delta x)^3} \\
u_m^{n+1} &= \frac{1}{4}(\bar{u}_{m+1}^{n+1} + 2\bar{u}_m^{n+1} + \bar{u}_{m-1}^{n+1}).
\end{aligned}$$

Similarly,

$$\begin{aligned}
\bar{g} &= 1 - \frac{a\lambda}{2}[e^{i\theta} - e^{-i\theta}] + \frac{1}{2}a^2\lambda^2[e^{i\theta} + e^{-i\theta} - 2] \\
&\quad - \frac{1}{12}a^3\lambda^3[e^{2i\theta} - 2e^{i\theta} + 2e^{-i\theta} - e^{-2i\theta}] \\
&= 1 - \frac{a\lambda}{2} \cdot 2i\sin\theta + \frac{1}{2}a^2\lambda^2(2\cos\theta - 2) - \frac{1}{12}a^3\lambda^3 \cdot 4i\sin\theta(\cos\theta - 1) \\
&= 1 - ia\lambda\sin\theta + a^2\lambda^2(\cos\theta - 1) - \frac{1}{3}ia^3\lambda^3\sin\theta(\cos\theta - 1) \\
&= [1 - 2a^2\lambda^2\sin^2\frac{\theta}{2}] + i[-a\lambda\sin\theta + \frac{2}{3}a^3\lambda^3\sin\theta\sin^2\frac{\theta}{2}]
\end{aligned}$$

$$\begin{aligned}
|\bar{g}|^2 &= 1 + 4a^4\lambda^4\sin^4\frac{\theta}{2} - 4a^2\lambda^2\sin^2\frac{\theta}{2} + a^2\lambda^2\sin^2\theta + \frac{4}{9}a^6\lambda^6\sin^2\theta\sin^4\frac{\theta}{2} - \frac{4}{3}a^4\lambda^4\sin^2\theta\sin^2\frac{\theta}{2} \\
&= 1 + a^2\lambda^2[\sin^2\theta - 4\sin^2\frac{\theta}{2}] + a^4\lambda^4[4\sin^4\frac{\theta}{2} - \frac{4}{3}\sin^2\theta\sin^2\frac{\theta}{2}] + \frac{4}{9}a^6\lambda^6\sin^2\theta\sin^4\frac{\theta}{2}
\end{aligned}$$

and $g = \bar{g}\cos^2\frac{1}{2}\theta$. One can numerically show the corresponding stable condition is $|a\lambda| \leq 1$, where $|g| = 1$ at $\theta = 2N\pi$ (check figure 5.3)

Figure 5.4 shows the set of points of $g(\theta)$s for $|a\lambda| = 1$. The blue curve is the unit circle. The red curve represents the $g(\theta)$ for the semi-discrete scheme without smoothing operator, while the green curve represents the $g(\theta)$ for the semi-discrete scheme with smoothing. The green curve touches at 1 because $g(0) = 1$. Similarly, comparison confirms that the smooth filter case covers a smaller region; thus it

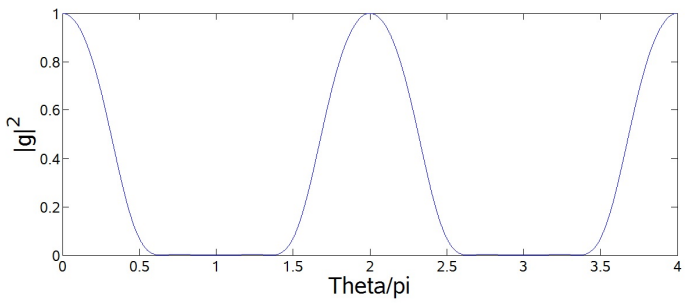

Figure 5.3 θ vs $|g|^2$ for $|a\lambda| = 1$.

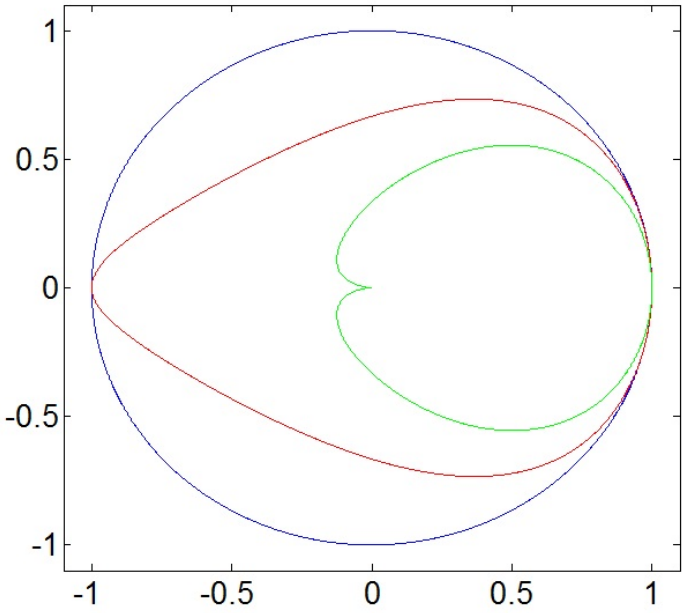

Figure 5.4 The images of $g(\theta)$. The blue curve is the unit circle. The red curve represent the $g(\theta)$ for semi-discrete scheme without smoothing operator, while the green curve represent the $g(\theta)$ for semi-discrete scheme with smoothing operator.

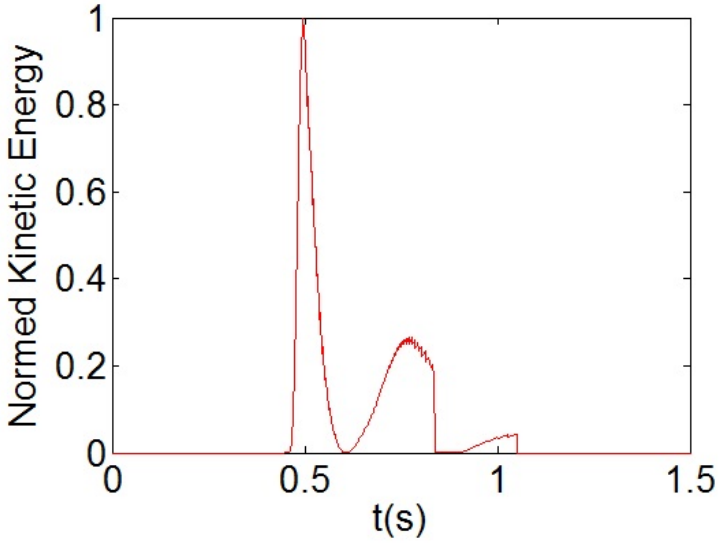

Figure 5.5 The evolution of normed kinetic energy with moving averages.

improves the stability. In particular, it follows that stability is obtained for the linearized frozen coefficient momentum equation of the BSR model when the ratio of space to time increments satisfy certain estimates, and this can be shown to hold true for the continuity equation as well.

The linearized frozen coefficient continuity equation $\rho_t + a\rho_x + b\rho = 0$ has the same basic form as the momentum equation. Therefore, it follows from Theorem 5.1 that the same stability requirement applies.

In addition, one can also show the stability effect of the moving average by studying of the evolution of kinetic energy. Take the numerical experiment of a single tap in Chapter 4 for example. Using $\sum_y \frac{1}{2}\rho(t)u^2(t)$ as a representation of the kinetic energy, one can norm this by its own maximum, i.e. $\frac{\sum_y \rho(t)u^2(t)}{\mathbf{Max}_t(\sum_y \rho(t)u^2(t))}$. Figure 5.5 and figure 5.6 shows the evolution of normed kinetic energy with and without the

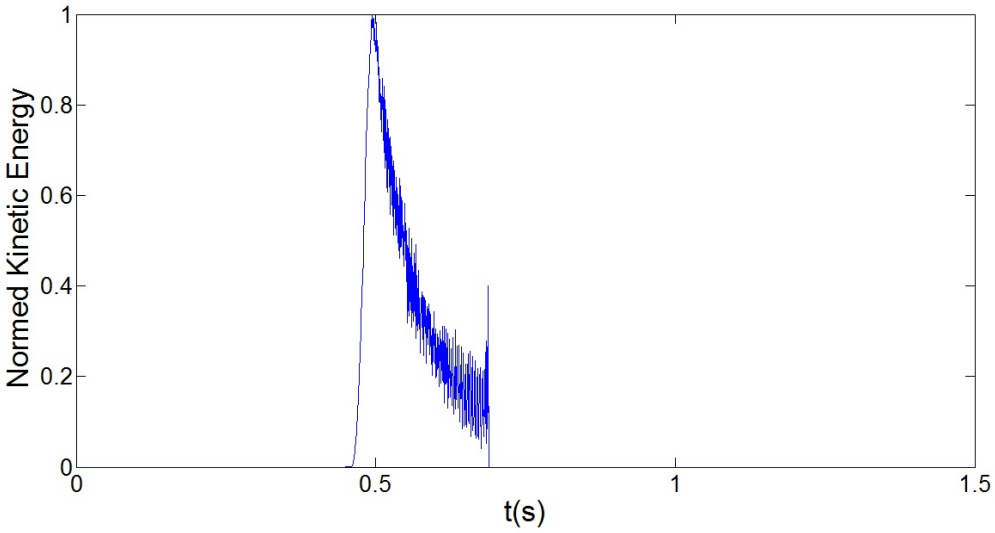

Figure 5.6 The evolution of normed kinetic energy without moving averages.

moving average, respectively. Figure 5.6 shows very large and rapid oscillations and this causes the numerical scheme to break down after 0.7s. This is because the spatial derivatives of u and ρ become extremely large due to the rapid oscillations.

In summary, the stability of the semi-discrete scheme for the linearized BSR momentum and the linearized BSR continuity equation are studied. The corresponding CFL condition is found and it is shown that with the smoothing moving average filter, the stability is enhanced. In general, very little information is available on the stability of general nonlinear discretized schemes. Within the framework of the von Neumann method it can be said that the stability of the linearized equations, with frozen coefficients, is necessary for the stability of the non-linear form but that it is certainly not sufficient. Products of the form $u\frac{\partial u}{\partial x}$ will generate high frequency waves which, through a combination of the Fourier modes on a finite mesh, will reappear as low-frequency waves and could deteriorate the solutions. The most frequently applied method consists in adding higher-order terms which provide additional dissipation in order to damp the nonlinear instabilities without affecting the accuracy. One could

also try to find the CFL condition for the linearized scheme, and then restrict the condition to back-test the numerical simulation until one finds a convergent scheme. The stability of the numerical scheme implemented in this dissertation is achieved with the addition of a smoothing moving average filter.

Finally, it should be observed that based upon the above results, $|u\lambda| \leq 1$ seems like a good working requirement for stability in the nonlinear case, and this is precisely what has been used for the numerical solutions.

CHAPTER 6

CONCLUSION AND FUTURE WORK

In this chapter, a summary of the methods employed and results obtained in this dissertation research will be presented. Future work on BSR system is also planned in the direction of extending the numerical scheme and performing more detailed analysis of the BSR model and its solutions, including possible traveling wave solutions and their stability and the possibility of specialized solution sets such as attractors. All of which should contribute to a much better understanding of granular flow phenomena.

1 The infinite-dimensional BSR dynamical model for granular flow is proved to be globally well-posed under conditions that apply to many granular flow and other types of physical dynamical systems. This appears to be the first such rigorous result of its kind for reasonably effective continuum models for particulate dynamics.

2 The semidiscrete numerical scheme for solving the 1D BSR model produces results that have been shown to compare well with very accurate DEM simulations.

3 The main well-posedness results for the BSR model shall be sharpened and generalized to apply to a wider range of flow fields.

4 The semidiscrete numerical method developed for the 1D BSR model will be extended to three-dimensional space and used to develop software for granular flow research. In particular, it will include a means for automatically dealing with the stiffness of a variety of problems, which produces the extreme oscillations in the numerical output seen in our examples.

5 Rigorous proofs in higher dimensions for the stability and other properties will be obtained for the semidiscrete numerical scheme.

6 Some of the analytical tools used for well-posedness will be used to investigate special types of wave-like solutions of the BSR equations and determine their stability. In particular, the focus shall be on the existence, stability and dynamics of traveling wave solutions.

7 The complete integrability results in the literature for the perfectly elastic 1D BSR model shall be generalized to include certain types of perfectly elastic higher dimensional cases.

APPENDIX A

DERIVATION OF LOCAL WAVE SPEED

In this appendix, a novel derivation of local wave speed with respect to BSR system is introduced and computed directly using the semi-discrete method for numerically solving the BSR system for some single tap numerical simulations.

Ignoring the gravitational and inertial forces, the BSR momentum equation turns out to be

$$u_t + uu_x = F(x,t) = \frac{\partial}{\partial x}\int_{x_0}^{x} F(\xi,t)d\xi. \tag{A.1}$$

Define

$$\Phi = \int_{x_0}^{x} F(\xi,t)d\xi. \tag{A.2}$$

Considering a small steady perturbation, it is easy to get

$$\frac{\partial}{\partial x}\{\frac{u^2}{2} + \int_{x_0}^{x} F(\xi,t_s)d\xi\} = 0, \tag{A.3}$$

i.e.,

$$\frac{\partial}{\partial x}(\frac{u^2}{2} + \Phi_s) = 0, \tag{A.4}$$

while the continuity equation yields

$$\rho u = \textbf{const.} \tag{A.5}$$

Hence, for a small perturbation, one obtains

$$\rho u = (\rho + \delta\rho)(u + \delta u) \tag{A.6}$$

$$\Phi - (\Phi + \delta\Phi) = \frac{1}{2}[(u + \delta u)^2 - u^2] = \frac{1}{2}[2u\delta u + (\delta u)^2] \tag{A.7}$$

Ignoring higher order terms, the following estimates are obtained

$$\rho\delta u = -u\delta\rho \tag{A.8}$$

$$u\delta u = -\delta\Phi \tag{A.9}$$

Combining the above two equations, (A.8) and (A.9), one gets

$$u^2 = \rho\frac{\delta\Phi}{\delta\rho} \tag{A.10}$$

In the limit at $\delta \to 0$, the speed of propagation is

$$u^2 = \frac{d\Phi}{d(\log\rho)} \tag{A.11}$$

Hence, to approximate the local wave speed at any time or position, the equation

$$c^2 \simeq \frac{d\Phi}{d(\log\rho)}. \tag{A.12}$$

appears to be a handy tool. As described above, as long as one has the data of the local variation of density and the local variation of the force, one should be able to compute the local wave speed at any time and any position. The following simulation results are for the single tap of a column of particles (spheres) with $a = 1.0d$ and $f = 10Hz$, where the tap is initiated at $t = 0.45s$. Figure (A.1) shows the local wave speed at different representative times following a top sphere trajectory and Figure (A.2) shows the local wave speed at some representative times following a middle sphere trajectory. The calculations of wave speeds is made over the time period from 0.4s-0.9s.

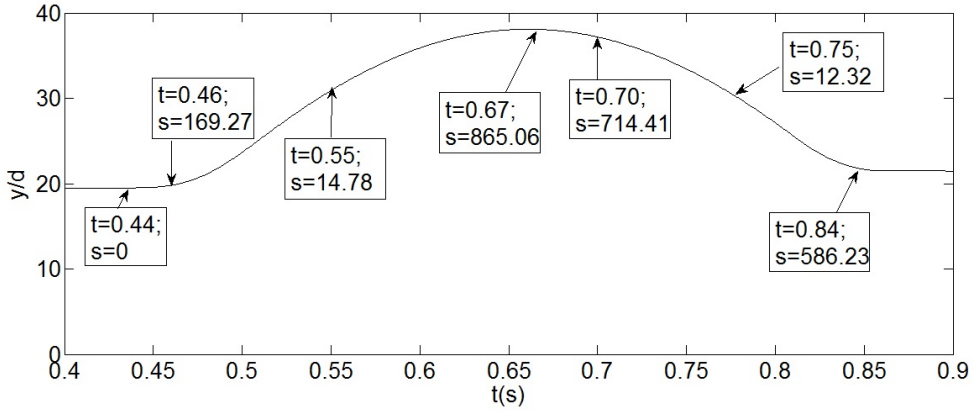

Figure A.1 A top trajectory and the corresponding local wave speeds for a single tap with $a = 1.0d$ and $f = 10Hz$ at some representative times. s has units m/s.

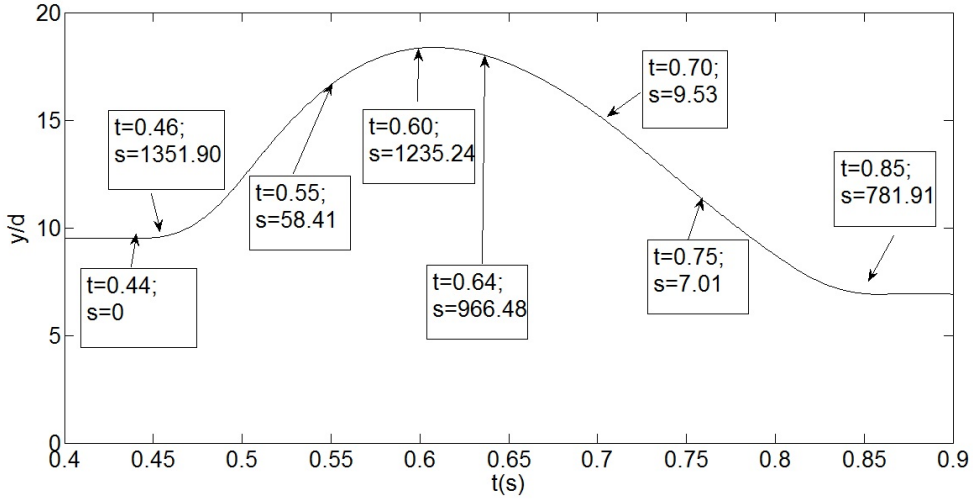

Figure A.2 A middle sphere trajectory and the corresponding local wave speeds for a single tap with $a = 1.0d$ and $f = 10Hz$ at some representative times. s has units m/s .

APPENDIX B

REVIEW OF THE RUNGE-KUTTA METHOD FOR SOLVING COUPLED FIRST ORDER DIFFERENTIAL EQUATIONS

This review is included for solutions in the case of two coupled first order differential equations mainly as a handy comparison with the slightly modified approach moving average approach that is actually used in the dissertation. The illustrative equations are taken to be the following system:

$$\frac{dx}{dt} = f(t, x, y)$$

$$\frac{dy}{dt} = g(t, x, y)$$

The solution can be obtained by the Runge–Kutta (R-K) method, correct to third order terms in t, using

$$k_1 = f(t_n, x_n, y_n)\Delta t$$

$$l_1 = g(t_n, x_n, y_n)\Delta t$$

$$k_2 = f(t_n + \frac{\Delta t}{2}, x_n + \frac{k_1}{2}, y_n + \frac{l_1}{2})\Delta t$$

$$l_2 = g(t_n + \frac{\Delta t}{2}, x_n + \frac{k_1}{2}, y_n + \frac{l_1}{2})\Delta t$$

$$k_3 = f(t_n + \Delta t, x_n - k_1 + 2k_2, y_n - l_1 + 2l_2)\Delta t \tag{B.1}$$

$$l_3 = g(t_n + \Delta t, x_n - k_1 + 2k_2, y_n - l_1 + 2l_2)\Delta t \tag{B.2}$$

The the numerical results based on given increments are:

$$x_{n+1} = x_n + \frac{1}{6}(k_1 + 4k_2 + k_3) \tag{B.3}$$

$$y_{n+1} = y_n + \frac{1}{6}(l_1 + 4l_2 + l_3), \tag{B.4}$$

where n represents the time step.

The coupled BSR system has the form

$$\frac{d\rho}{dt} = F(\rho, u, \rho_y, u_y)$$

$$\frac{du}{dt} = G(t, \rho, u, u_y),$$

which can be obtained by the R-K method, correct to third order terms in t, using

$$K_1 = F\left(\rho_n, u_n, (\rho_n)_y, (u_n)_y\right)\Delta t$$

$$L_1 = G\left(t_n, \rho_n, u_n, (u_n)_y\right)\Delta t$$

$$K_2 = F\left(\rho_n + \frac{K_1}{2}, u_n + \frac{L_1}{2}, (\rho_n + \frac{K_1}{2})_y, (u_n + \frac{L_1}{2})_y\right)\Delta t$$

$$L_2 = G\left(t_n + \frac{\Delta t}{2}, \rho_n + \frac{K_1}{2}, u_n + \frac{L_1}{2}, (u_n + \frac{L_1}{2})_y\right)\Delta t$$

$$K_3 = F\left(\rho_n - K_1 + 2K_2, u_n - L_1 + 2L_2, (\rho_n - K_1 + 2K_2)_y, (u_n - L_1 + 2L_2)_y\right)\Delta t$$

$$L_3 = G\left(t_n + \Delta t, \rho_n - K_1 + 2K_2, u_n - L_1 + 2L_2, (u_n - L_1 + 2L_2)_y\right)\Delta t, \qquad \text{(B.5)}$$

where the F and G is used to denote the right hand side of the BSR continuity and momentum equations.

As a result, the numerical increment based results are as follows:

$$\rho_{n+1} = \rho_n + \frac{K_1 + 4K_2 + K_3}{6},$$

$$u_{n+1} = u_n + \frac{L_1 + 4L_2 + L_3}{6}.$$

APPENDIX C

A PSEUDOCODE FOR THE NUMERICAL SCHEME

The following is a pseudo code for the numerical scheme.

```
1  Clear previous data in the work-space;
2  Set the grid mesh;
3  Set the Parameters and Initialize the data;
4  Set the upper and lower bounds to satisfy CFL condition.
5
6  Goto the time loop:
7  update the external force term in the momentum equation at t;
8  update the interaction force integral in the momentum ...
       equation at t;
9  update the right hand side of the continuity equation at t;
10 update the external force term in the momentum equation at ...
       t+dt/2;
11 update the interaction force integral in the momentum ...
       equation at t+dt/2;
12 update the right hand side of the continuity equation at ...
       t+dt/2;
13 update the external force term in the momentum equation at ...
       t+dt;
```

```
14 update the interaction force integral in the momentum ...
     equation at t+dt;
15 update the right hand side of the continuity equation at t+dt;
16 apply the Runge–Kutta formula to calculate velocity as new ...
     velocity;
17 apply the Runge–Kutta formula to calculate density as new ...
     density;
18 apply the moving average to the velocity field;
19 apply the moving average to the density field;
20 integrate the new positions using the velocity information;
21 end time loop.
22
23 plot ;
```

BIBLIOGRAPHY

[1] R. Adams. *Sobolev Spaces*. Academic Press, Boston, MA, 1975.

[2] K. Atkinson, W. Han, and D. Stewart. *Numerical Solution of Ordinary Differential Equations*. John Wiley & Sons, Hoboken, NJ, 2009.

[3] R.A. Bagnold. *The Physics of Blown Sand and Desert Dunes*. London: Methuen, 1941.

[4] D. Blackmore, A. Rosato, X. Tricoche, K. Urban, and V. Ratnaswamy. Tapping dynamics for a column of particles and beyond. *Journal of Mechanics of Materials and Structures*, 6(1-4):71–86, 2011.

[5] D. Blackmore, R. Samulyak, and A. Rosato. New mathematical model for particle flow dynamics. *J. Nonlin. Math. Phys.*, 6:198–221, 1999.

[6] D. Blackmore, K. Urban, and A. Rosato. Integrability analysis of regular and fractional Blackmore-Samulyak-Rosato fields. *Condensed Matter Phys.*, 13:43403: 1–7, 2010.

[7] J. Bougie, S.J. Moon, J.B. Swift, and H.L. Swinney. Shocks in vertically oscillated granular layers. *Phys. Rev. E*, 81:061301, 2010.

[8] C. Brennen, S. Ghosh, and C. Wassgren. Vertical oscillation of a bed of granular material. *Trans. ASME*, 63:156–161, 1996.

[9] J.A. Carrillo, T. Poschel, and C. Saluena. Granular hydrodynamics and pattern formation in vertically oscillated granular disk layers. *J. Fluid Mech.*, 597, 2008.

[10] C. Cercignani. Small data existence for the enskog equation in L^1. *J. Stat. Phys.*, 51, 1988.

[11] M.P. Ciamarra, M.D. Vizia, A. Fierro, M. Tarzia, A. Coniglio, and M. Nicodemi. Granular species segregation under vertical tapping: Effects of size, density, friction, and shaking amplitude. *Phys. Rev. E*, 96(5), 2006.

[12] A. Clark, L. Kondic, and R.P. Behringer. Particle scale dynamics in granular impact. *Phys. Rev. Lett.*, 109:238302, 2012.

[13] E. Coddington and N. Levinson. *Theory of Ordinary Differential Equations*. Krieger Publ., Malabar, FL, 1984.

[14] K. Courant, R.and Friedrichs and H. Lewy. On the partial difference equations of mathematical physics. *IBM Journal of Research and Development*, 11 (2), 1928.

[15] C. Daraio, V. Nesterenko, E. Herbold, and S. Jin. Tunability of solitary wave properties in one dimensional strongly nonlinear phononic crystals. *Phys. Rev. E*, 73:026610, 2006.

[16] M. Esteban and B. Perthame. On the modified enskog equation for elastic and inelastic collisions. models with spin. *Ann. Inst. H. Poincare Anal. Non Lineaire*, 8, 1991.

[17] E. Falcon, C. Laroche, S. Fauve, and C. Coste. Collision of a 1-D column of beads with a wall. *Eur. Phys. J.*, B5:111–131, 1998.

[18] E. Fermi, J. Pasta, and S. Ulam. Studies of nonlinear problems. *Document LA-1940*, 1955.

[19] S-Y. Ha and S. Noh. New a priori estimate for Boltzmann-Enskog equation. *Nonlinearity*, 19, 2006.

[20] P. Hartman. *Ordinary Differential Equations*. Wiley, New York, NY, 1964.

[21] G. Klinzing, F. Rizk, R.D. Marcus, and L.S. Leung. *Pneumatic conveying of solids - atheoretical and practical approach.* Springer, Dordrecht, Neitherland, 2010.

[22] L. Kondic, A. Goullet, C.S. O'Hern, M. Kramar, K. Mischaikow, and R.P. Behringer. Topology of force networks in compressed granular media. *Europhys. Lett.*, 97, 2012.

[23] M. Kramar, A. Goullet, L. Kondic, and K. Mischaikow. Persistence of force networks in compressed granular media. *Phys. Rev. E*, 87, 2013.

[24] M. Kramar, A. Goullet, L. Kondic, and K. Mischaikow. Evolution of force networks in dense particulate media. *Phys. Rev. E*, 90, 2014.

[25] M. Kramar, A. Goullet, L. Kondic, and K. Mischaikow. Quantifying force networks in particular systems. *Physica D*, 283, 2014.

[26] H.O. Kreiss. Initial boundary value problems for hyperbolic systems. *Comm. Pure Appl. Math.*, 23, 1970.

[27] P.D. Lax and R.D. Richtmyer. Survey of the stability of linear finite difference equations. *Comm. Pure Appl. Math.*, 9, 1956.

[28] A. Levy and H. Kalman. *Handbook of conveying and handling of particulate solids*. 2001.

[29] M.Y. Louge. Impact parameter chart for spheres. *Eur. Phys. J.*, 1999.

[30] G. Lumay, S. Darbolo, O. Gerasymov, and N. Vanderwalle. Experimental study of a vertical column of grains submitted to a series of impulses. *Eur. Phys. J.*, E36:13016, 2013.

[31] R. McOwen. *Partial Differential Equations : Methods and Applications.* Prentice Hall, Upper Saddle River, New Jersey, 1996.

[32] E.R. Merrow. *Linking R & D to problems experienced in solids processing.* Rand Corporation, Santa Monica, CA, 1984.

[33] G. Metcalfe, S.G.K. Tennakoon, L. Kondic, D.G. Schaeffer, and R.P. Behringer. Granular friction, coulomb failure, and fluid-solid transition for horizontally shaken granular materials. *Phys. Rev. E*, 65:031302–1 – 031302–15, 2002.

[34] R.D. Mindlin and H. Deresiewicz. Elastic spheres in contact under varying oblique forces. *J. Appl. Mech.*, 20, 1953.

[35] R.M. Miura, C.S. Gardner, and M.D. Kruskal. Korteweg de Vries equation and generalizations. II. existence of conservation laws and constants of motion. *J. Mathematical Phys.*, 9 (8):12041209, 1968.

[36] V. Nesterenko. Propagation of nonlinear compression pulses in granular media. *J. Appl. Mech. Tech. Phys.*, 24:5:733–743, 1984.

[37] V.F. Nesterenko, C. Daraio, E.B. Herbold, and S. Jin. Anomalous wave reflection at the interface of two strongly nonlinear granular media. *Phys. Rev. Lett.*, 95:15:158702, 2005.

[38] J. Polewczak. Global existence in L^1 for the generalized Enskog equation. *J. Stat. Phys.*, 59, 1990.

[39] A. Ralston. Runge–Kutta methods with minimum error bounds. *Math. Comp.*, 16:431–437, 1962.

[40] M. Renardy and R. Rogers. *An Introduction to Partial Differential Equations.* Springer-Verlag, New York, NY, 1993.

[41] A. Rosato, O. Dybenko, D.J. Horntrop, V. Ratnaswamy, and L. Kondic. Microstructure evolution in density relaxation by tapping. *Phys. Rev. E*, 81:061301, 2010.

[42] A.D. Rosato, D. Blackmore, X.M. Tricoche, K. Urban, and L. Zuo. Dynamical systems model and discrete element simulations of a tapped granular column. *AIP Conf. Proc.*, 1542, 317, 2013.

[43] S. Sen and M. Manciu. Discrete hertzian chains and solitons. *Physica A*, 268:644–649, 1999.

[44] S. Sen and M. Manciu. Solitary wave dynamics in generalized hertz chains: An improved solution of the equation of motion. *Phys. Rev. E*, 64:056605– 1 – 056605–4, 2001.

[45] H. Shintani and K. Toemeda. Stability of difference schemes for nonsymmetric linear hyperbolic systems with variable coefficients. *Hiroshima Math. J.*, 7, 1977.

[46] E.M. Stein and G. Weiss. *Introduction to Fourier Analysis on Euclidean Spaces*. Princeton University Press, Princeton, NJ, 1971.

[47] J.C. Stirkwerda. *Finite Difference Schemes and Particle Differential Equations*. SIAM, 2004.

[48] M. Suzuki, H. Sato, M. Hasegawa, and M. Hirota. Effect of size distribution on tapping properties of fine powder. *Powder Technology*, 118, 2001.

[49] E. Tadmor. Stability analysis of finite-difference, pseudospectral and fourier-galerkin approximations for time-dependent problems. *SIAM Rev.*, 29, 1987.

[50] M. Takahashi and S. Suzuki. Numerical analysis of tapping behavior of ceramic powders. *Ceramic Bulletin*, 65, 1986.

[51] S.G.K. Tennakoon, L. Kondic, and R.P. Behringer. Onset of a flow in horizontally vibrated granular bed convection by horizontal shearing. *Europhysics Lett.*, 45:470–475, 1999.

[52] G. Toscani and N. Bellomo. The Boltzmann-Enskog equation in the whole space R^3. Some global existence, uniqueness and stability results. *Comput. Math. Appl.*, 13, 1987.

[53] L.N. Trefethen. *Finite Difference and Spectral Methods for Ordinary and Partial Differential Equations*. Cornell University, Ithaca, NY, 1996.

[54] O.R. Walton. *Numerical Simulation of Inelastic, Frictional Particle-particle Interactions, in Particulate Two-Phase Flow*. Butterworths, Boston, MA, 1992.

[55] O.R. Walton and R.L. Braun. Stress calculations for assemblies of inelastic spheres in uniform shear. *Acta Mechanica*, 63 (1-4), 1986.

[56] M. Yamaguti and T. Nogi. An algebra of pseudo-difference schemes and its application. *Publ. RIMS Kyoto Univ. Ser. A*, 3, 1967.

[57] N.J. Zabusky and M.D. Kruskal. Interaction of solitons in a collisionless plasma and the recurrence of initial states. *Phys. Rev. Lett.*, 15 (6):240243, 1965.